ANALYSIS AND OPTIMIZATION OF A SMALL SCALE SOLAR ORGANIC RANKINE CYCLE SYSTEM FOR POWER GENERATION

by

Umut Soysal

B.S., Mechanical Engineering, Boğaziçi University, 2014

Submitted to the Institute for Graduate Studies in
Science and Engineering in partial fulfillment of
the requirements for the degree of
Master of Science

Graduate Program in Mechanical Engineering

Boğaziçi University

2017

ACKNOWLEDGEMENTS

I would like to thank my thesis advisor Assoc. Prof. Hasan Bedir and Prof. Gunay Anlaş. Their continuous support, help and tolerance allowed me to finish my studies. Their wisdom and personality had a great influence on me and gave me courage to follow my career path.

I would like thank Emre Sezerkan and Onur Kardas for their company during my studies. It was a great pleasure to work with them from the beginning of the establishment of BURET laboratory to the completion of the thesis study. I also thank my fellow labmates Mehdi Nabati, Hamed Shafiei and Alpay Asma for their cooperation and friendship.

I would also like to thank my housemates, Mert Bacak and Kaan Can for their support during my thesis writing period. They helped me to endure my hard times and showed me the value of having good friends when facing any hardship or sharing good times in the life.

Finally, I am grateful for having such a great family. I could not accomplish this study and many other things without their unconditioned love, patience and support.

Umut Soysal

ABSTRACT

ANALYSIS AND OPTIMIZATION OF A SMALL SCALE SOLAR ORGANIC RANKINE CYCLE SYSTEM FOR POWER GENERATION

In this study, a numerical model of a small scale concentrated solar power system is designed for Istanbul conditions and the annual performance of the system is evaluated. As a collector system, a thermal model of parabolic trough collectors are modeled and the heat output of the collector system is compared with experimental data. For the power block, a steady state organic Rankine cycle (ORC) system is used. ORC system is composed of an evaporator, a condenser, a pump and an expander. For the working fluid R245fa is chosen and whole system is modeled in MATLAB environment. Single tank thermocline storage model is implemented to observe the performance increase of the system with a proper thermal storage system. Using meteorological data, the annual performance of the designed system is estimated. Optimum values for mass flow rates, cycle pressures and required collector area is studied.

ÖZET

KÜÇÜK ÖLÇEKLİ SOLAR ORGANİK RANKİNE ÇEVRİMİ İLE GÜÇ ÜRETİMİ ANALİZİ VE OPTİMİZASYONU

Bu çalışmada, konsantre güneş enerjisi teknolojisi ile enerji sağlanan küçük ölçekli organik Rankine çevrimi sistemi modellemesi yapıldı. Çevrim sisteminindeki akışkan gazı ısıtmak için kullanılan güneş kolektörlerinin modellemesi yapildi ve performansları 2 boyutlu olarak termal direnç yöntemi kullanılarak hesaplandi. Oluşturulan model, literatürde kabul görmüş test sonuçlarıyla doğrulandı. Organik Rankine çevriminin termodinamik tasarımı yapıldı. Sistemde kullanılacak olan akışkan R245fa olarak belirlendi ve sistem ideal koşullarda 10 kW güç üretecek şekilde boyutlandırıldı. İstanbula ait saatlik meteoroloji verileri kullanılarak sistem yıllık olarak simüle edildi. Bu çalışma ile çevrim sisteminin tasarım koşullarının dışarısında nasıl çalışacağı ve değişen hava koşullarının sistemin performansını nasıl etkileyeceği araştırıldı.

TABLE OF CONTENTS

ACKNOWLEDGEMENTS . . . iii
ABSTRACT . . . iv
ÖZET . . . v
LIST OF FIGURES . . . viii
LIST OF TABLES . . . x
LIST OF SYMBOLS . . . xi
LIST OF ACRONYMS/ABBREVIATIONS . . . xiii
1. INTRODUCTION . . . 1
1.1. CSP Technology Overview . . . 1
1.2. Low Temperature Power Cycles . . . 5
1.3. Current State in Turkey . . . 8
2. OBJECTIVES . . . 9
3. BACKGROUND . . . 10
3.1. Parabolic Trough Geometry . . . 10
3.2. Thermal Storage Systems for CSP . . . 12
3.2.1. Sensible Heat Storage . . . 14
3.2.2. Latent Heat storage . . . 15
3.2.3. Chemical Energy storage . . . 16
3.3. Fluid Selection for Organic Rankine Cycles . . . 16
3.4. Radiation Definitions . . . 19
4. THERMODYNAMIC MODEL METHODOLOGY . . . 21
4.1. System Model Description . . . 21
4.2. Parabolic Collector Model . . . 21
4.2.1. Solution method for Thermal Resistance Model . . . 29
4.2.2. Model Validation . . . 31
4.3. ORC system model . . . 34
4.3.1. ORC fluid Pump . . . 35
4.3.2. Evaporator . . . 35
4.3.3. Expander . . . 36

4.3.4. Condenser 36
4.4. Single Tank Thermal Storage Model 37
4.5. Daily Simulation 39
5. RESULTS AND DISCUSSION 42
5.1. Collector area sizing for power block 47
5.2. Effect of the HTF flow rate on daily performance 49
5.3. Effect of the evaporation pressure on daily performance 49
5.4. Effect of the thermal storage tank on the daily work output 50
5.5. Thermal Storage Tank Volume sizing for power block 51
6. CONCLUSION 54
REFERENCES 55

LIST OF FIGURES

1.1	Parabolic Trough Collectors [2].	2
1.2	Linear Fresnel Collectors [2].	3
1.3	Solar Tower [2].	3
1.4	Dish Stirling engine.	4
1.5	Basic ORC cycle (left), ORC with a regenerator (right).	6
1.6	Installed capacity shares of ORC systems.	7
3.1	Collector Geometry [15].	10
3.2	Collector cross-section.	11
3.3	Rim Angle for the Collector.	12
3.4	Classification of storage systems.	13
3.5	T-s diagram for fluids, (a) wet, (b) isentropic, (c) dry.	17
3.6	Selection procedure of the working fluid in a solar ORC [25].	18
3.7	DNI vs GHI values for fixed plane for Antalya in June.	20
4.1	Organic Rankine Cycle	21
4.2	T-s Diagram for R254fa	22
4.3	Parts of a heat collection element (HCE) and control volume used for the heat transfer analysis. Adapted from [30].	22
4.4	Energy Balance in receiver cross section	22
4.5	Thermal resistance model of the receiver in radial direction	23
4.6	Incident angle modifier for LS-2 collector	29
4.7	Solution method for Solving Thermal Resistance Method.	30
4.8	Calculation of collector outlet temperature.	31
4.9	Efficiency of cermet receiver with vacuum annulus.	32
4.10	Thermal loss of cermet receiver with vacuum annulus.	32
4.11	Efficiency of cermet receiver with air annulus.	33
4.12	Thermal Loss of cermet receiver with vacuum annulus.	33
4.13	ORC cycle diagram.	34
4.14	Thermocline Storage Tank Model.	37

4.15	Temperature distribution in different layers of the tank.	39
4.16	Monthly water and air temperatures of Istanbul.	41
5.1	Daily irradiation and collector output temperature in January. . .	42
5.2	Daily irradiation and collector output temperature in February. . .	43
5.3	Daily irradiation and collector output temperature in March. . . .	43
5.4	Daily irradiation and collector output temperature in April.	43
5.5	Daily irradiation and collector output temperature in May.	44
5.6	Daily irradiation and collector output temperature in June.	44
5.7	Daily irradiation and collector output temperature in July.	44
5.8	Daily irradiation and collector output temperature in August. . .	45
5.9	Daily irradiation and collector output temperature in September. .	45
5.10	Daily irradiation and collector output temperature in October. . .	45
5.11	Daily irradiation and collector output temperature in November. .	46
5.12	Daily irradiation and collector output temperature in December. .	46
5.13	Effect of the solar field are on the cumulative work.	48
5.14	Effect of the solar field are on the cumulative work.	49
5.15	Variation of work output with change of working fluid mass flow rate.	50
5.16	Variation of work output with change of working fluid mass flow rate.	51
5.17	Performance of the base system without storage in July.	52
5.18	Performance of the base system with storage in July.	52
5.19	Effect of tank volume on the cumulative work.	53

LIST OF TABLES

1.1 Installed Capacities and Produced Electricity by Technology Type [3]. 4

3.1 Selected ORC fluids for CSP applications. 19

4.1 Heat Transfer Coefficients and Constants for Each Annulus Gas [35]. 26

4.2 Zhukauskas correlation coefficients. 28

4.3 Optical Efficiency Terms provided by Forristall [35]. 28

4.4 SEGS LS-2 Parabolic Trough Solar Collector Test Specifications [36] 34

4.5 Heat Transfer coefficients for a standard oil storage tank 40

5.1 Base ORC specifications for simulation. 42

5.2 Daily performance of base case system with 200 m^2 collector area. 47

5.3 Base ORC performance with different collector areas. 48

LIST OF SYMBOLS

a	Aperture width
b	Interaction coefficient
C_g	Concentrating ratio
c_p	Specific heat
D	Diameter
f	Focal length
fr	Friction coefficient
g	Gravitational acceleration
h	Enthalpy
K	Incident angle modifier
k	Conductivity
l	Length
Nu	Nusselt number
P	Pressure
Pa	Pascal
Pr	Prandtl number
Q	Heat energy
Ra	Rayleigh number
Re	Reynolds number
T	Temperature
U	Heat loss coefficient
V	Volume
α	Thermal diffusivity
β	Volumetric thermal expansion coefficient
γ	Ratio of specific heats for annulus gas
δ	Molecular diameter
ϵ	Emissivity

η	Efficiency
λ	Mean-free path between collision of a molecule
ρ	Density
θ_r	Rim angle

LIST OF ACRONYMS/ABBREVIATIONS

CSP	Concentrated Solar Power
DNI	Direct Normal Irradiation
DSG	Direct Steam Generation
GHI	Global Horizontal Irradiation
GWP	Global Warming Potential
HCE	Heat Collecting Element
HTF	Heat Transfer Fluid
ODP	Ozone Depleting Potential
ORC	Organic Rankine Cycle
PCM	Phase Change Materials
SEGS	Solar Thermal Energy Generation System
TES	Thermal Energy Storage
WF	Working Fluid

1. INTRODUCTION

Renewable and clean energy is definitely one of the biggest challenge of the human society for this century. Uneven distribution of the resources caused many conflicts among countries and created inequality between them. The one of the biggest source of energy, petroleum market is controlled by oligopoly therefore energy prices are largely effected by political situations which is very inconvenient. Scarcity of fossil energy sources forced world countries to alternative energy sources. Solar energy research and applications are boosted to overcome this problem and first solar thermal energy generations systems (SEGS) are built in California [1].

In 1990's sustainability concept is defined and the question about whether there is enough energy resources today slightly moved towards to whether there will enough energy in future. The cheap and efficient energy of all forms are investigated. Being the direct or indirect source of every type energy of the world, the Sun itself is the focus of both research and industrial operations. One of the methods for direct utilization of solar power is concentrated solar power technology.

1.1. CSP Technology Overview

Concentrating Solar Power (CSP) technologies concentrate sunlight to a certain zone to achieve high temperatures to operate a power cycle or simply deliver heat energy for domestic or industrial usage. The mirrors of the CSP systems reflect sunlight onto the focal point or the focal line where a receiver is placed which heats a heat transfer fluid (HTF) circulating inside. The HTF with high temperature is used to rotate a turbine to convert thermal energy to mechanical work. The final output of the cycle is usually electricity which is converted by a generator from the mechanical energy General layout of CSP plants is shown in Figure **??**.

CSP systems are generally built in utility-scale to supply electricity to grid. However they can be constructed in different scales from 10 kilowatts for domestic usage to

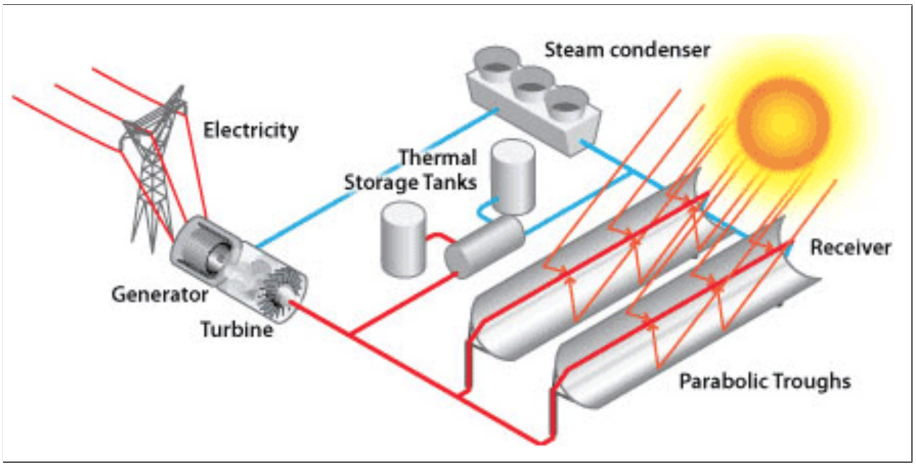

Figure 1.1. Parabolic Trough Collectors [2].

hundreds of megawatts for large scale electricity production. Main CSP configurations are:

- Parabolic Troughs
- Linear Fresnel Systems
- Solar Towers
- Dish Stirling Systems

Parabolic troughs are made of parabolic shaped metal or glass surface with a thermal receiver on the focal line of the surface. This geometry collects solar radiation onto the receiver and heats up the fluid inside the receiver. This systems are deployed in very different scales, from 10 kW to 500 MW and can be matched with different cycle applications.

First large scale application of parabolic trough systems is SEGS (Solar Electricity Generating Systems) plant installed in California by Luz International, Inc. in 1984 [1]. Until 1991 there 9 plants have been successively installed and total capacity is increased to 354 MW. The plants are still in operation.

In linear Fresnel reflector system, linear mirror strips mounted on trackers on the ground concentrate the Sun light onto a fixed absorber. The mirror strips can be flat or slightly curved. Main advantage of Fresnel systems over parabolic collector systems is

that due to their shapes, Fresnel mirrors are relatively cheaper then parabolic collectors. Total capacity built in Fresnel systems are approximately 179 MW in worldwide [3].

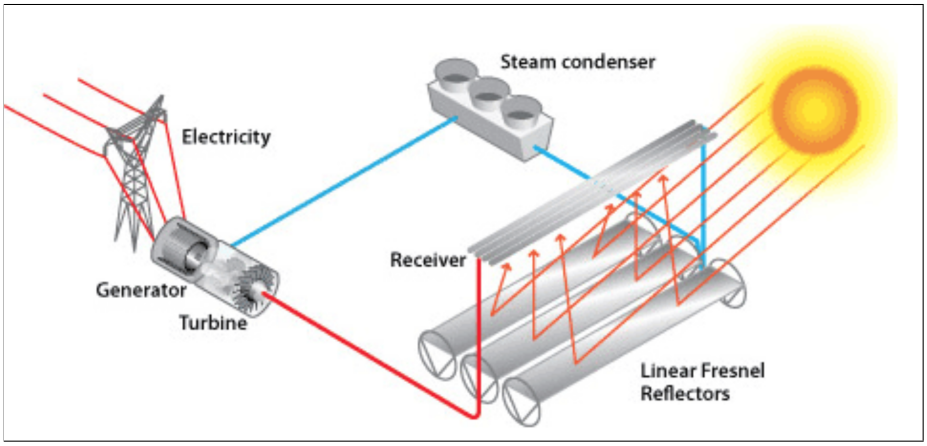

Figure 1.2. Linear Fresnel Collectors [2].

In power tower or solar tower type of concentrating solar power systems, a large number of flat mirrors which are placed around a tower, track the the Sun and reflect the sunlight onto a receiver at the top the tower. A HTF is circulated in the receiver to supply heat energy for the power cycle behind it. HTF in the power cycle can vary according to the temperature limits of the solar field. Water/steam can be used as the HTF. However for higher temperatures due to large collector field other fluids like water or molten salt may be used as HTF [2].

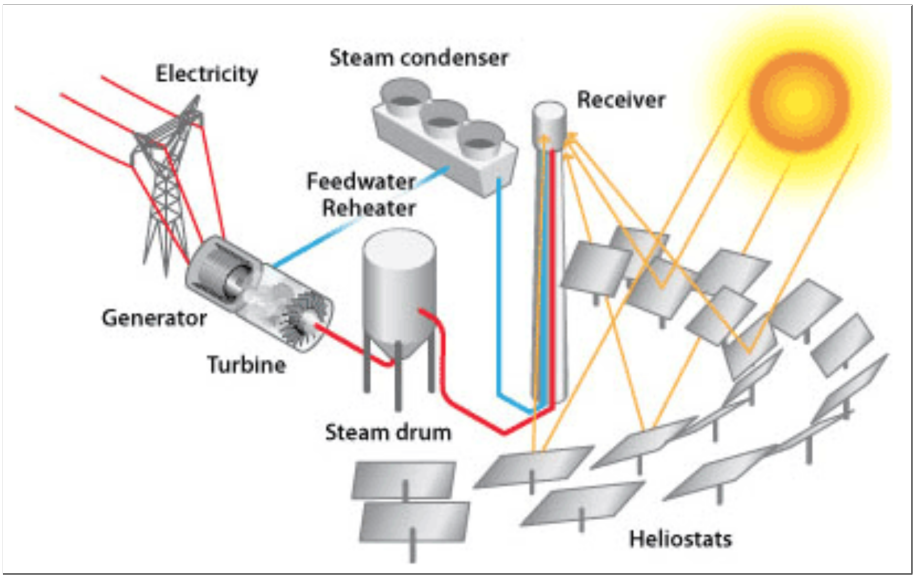

Figure 1.3. Solar Tower [2].

Dish/engine systems use a parabolic dish of mirrors to reflect the sunlight onto the focal point of the paraboloid surface. A small engine is placed in the focal point to convert the heat energy to mechanical work. The power output ranges of the Dish/Engines systems typically in the range of 3 to 25 kilowatts, however their efficiency is reported around 26%. In the current Dish/Engine systems the Stirling Engine is used as energy converter [4].

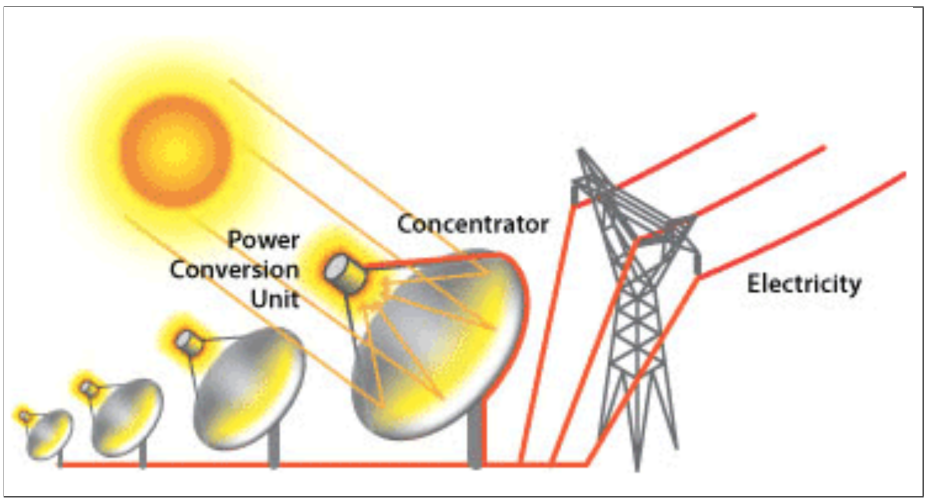

Figure 1.4. Dish Stirling engine.
citedoewebsite.

The installed capacities of different CSP technologies can be seen on Table 1.1. Up to 2016, the 85% of the installed capacity is made of parabolic trough. However in future, the percentage of the central receiver type systems are expected to increase.

Table 1.1. Installed Capacities and Produced Electricity by Technology Type [3].

Technology Type	No. of Plants	Installed Capacity (MW)	Annual Production (GWh)	Capacity Under construction
Parabolic Trough	73	4,115	10,000	719
Central Receiver	10	497	1300	410
Fresnel	8	179	350	180

All three CSP technology may be coupled with different power cycles to produce

electricity according to their output temperature. Scale of the plant is an important parameter for the temperature output of the solar collector field. For small scale CSP applications, low temperature power cycles might be beneficial to use.

1.2. Low Temperature Power Cycles

Rankine cycle is the most used thermodynamic cycle for power generation but it needs to be installed at large scales for high temperatures. Even the excess heat of the cycle have too much energy on it. To utilize thermal energy sources in low temperature, different cycles are developed and studied such as organic Rankine cycle, Kalina cycle, and Stirling cycle. These low temperature heat cycles can be deployed as bottoming cycle for high temperature plants or can be used as a standalone power generation systems.

In last two decades, organic Rankine cycle (ORC) has become a very popular research field and seen as a promising technology. Since the cycle uses fluids with lower evaporation temperature than water, the organic Rankine cycle may operate with low temperature heat sources such as Sun, biomass combustion, waste heat or geothermal heat sources. Organic Rankine cycles have been started to be studied in late 1970s and used in geothermal and waste heat applications.

Organic Rankine cycle systems are conceptually very similar to the conventional Rankine cycles which produce mechanical work from a turbine using high pressure fluid vapor. ORC systems differ from the Rankine cycle by its working fluid and being relatively simple and scalable design.

Basic ORC system is formed by an expander, a condenser, a pump and an evaporator, as shown in Figure 1.5. Often a regenerator or recuperator is implemented to the system to increase the efficiency. In some cycles, superheating process is applied to the system to further efficiency increase with a cost of adding a super heater to the system. According to the applications, system configurations may be changed slightly. Application areas of organic Rankine systems are:

- Biomass combustion
- Geothermal energy
- Solar Power plants
- Waste Heat recovery

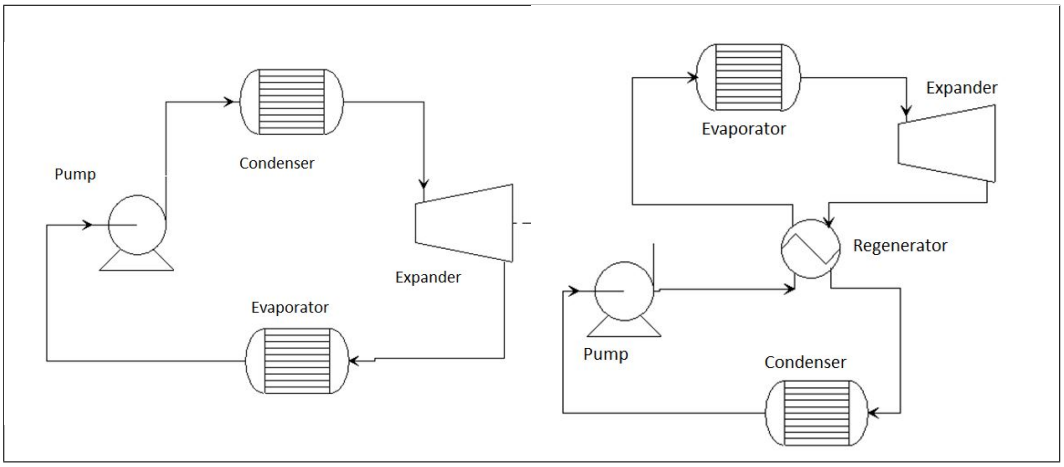

Figure 1.5. Basic ORC cycle (left), ORC with a regenerator (right).

In Biomass applications, combustion of the agricultural waste such as wood chips, straw or rice husk can be used as a heat source for the energy generation. Due to the lower energy density of these resources compared to fossil fuels and the need for local energy and heat supply around the plant site, ORC applications are suitable for energy generation from biomass combustion [5].

In Geothermal applications, brine temperature may vary from ambient temperature to 300 °C. If the source temperature is higher then 80°C the source can be exploited as a heat sources for ORC. For higher temperatures (more then 150°C), combined heat and power systems (CHP) become feasible to supply both power and hot water for any kind of usage [5].

Concentrating solar power is a promising application field for ORC systems especially in remote and off-grid areas. Largest installed plant with solar organic Rankine systems is Saguaro Power Plant located in Arizona which has a output capacity if 1.0 MW with 12% nominal efficiency at design point [4].

Waste Heat Recovery systems in heavy industry like cement iron or steel production provide great opportunities for ORC systems. Also ORC systems can be used as a bottoming cycle for gas turbines and internal combustion engines. There are various studies to implement ORC system in vehicle engines as well however possibly due to economical reasons, there is no widespread available commercial application of ORC systems in vehicles.

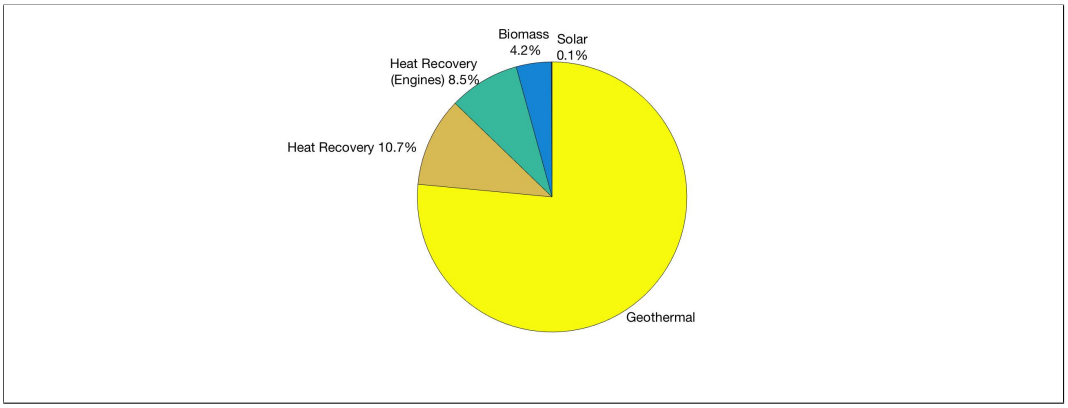

Figure 1.6. Installed capacity shares of ORC systems.

According to ORC World Map [6], total installed capacity of ORC systems around the world is reported as 2749.1 MWe in 563 plants. Geothermal energy is the biggest resource of energy with 76 % of the installed capacity.

Current research and development on ORC systems mainly focus on fluid selection, turbo machinery design, optimization, innovative cycle design like cascades cycles or multi-phase expansions cycles [5].

In literature there are several studies to investigate CSP-ORC systems for small scale applications. Orozs *et al.* [7] designed and developed a small scale solar organic Rankine cycle system for an off-grid application in Lesotho.

Freeman *et al.* made a comparative study between evacuated tube collectors with ORC cycle and photo voltaic systems on a roof of a standard house. He concluded that even for London conditions CSP applications might an option for household energy generation [8].

Wang *et al.* made a parametric study to observe effects of operation temperatures and pressures over the total efficiency with a CSP-ORC model with single tank storage [9].

He *et al.* made a similar study and made an annual simulation to determine optimum size for thermal storage system and found that heat transfer loss from the collector reduce significantly if receiver annulus is in vacuum. [10].

Pehlivanturk *et al.* modeled and studies and ORC cycle with propane boiler as an auxiliary heating system to determine performance of different collector systems [11].

1.3. Current State in Turkey

According to YEGM (Yenilenebilir Enerji Genel Müdürlüğü), Turkey has an average 7.2 hour insolation time with 3.6 kWh total energy value in a day. Even if the solar irradiation is abundant, no commercial concentrated solar power plant exists in Turkey. There is a pilot plant in Mersin built by Greenway [12]. The plant is designed for 5 MWt power with solar tower technology. The cycle operated in the plant is Direct Steam Generation (DSG) technology. Since the system is under development, the overall efficiency is not reported.

ORC systems in Turkey are implemented in geothermal applications over the last years. Up to 2016, there are 28 Geothermal powered ORC system are reported in Energy Outlook of Turkey [13].

2. OBJECTIVES

In this thesis, a 10 kW organic Rankine cycle system with parabolic trough collectors is modeled and simulated in Istanbul using daily meteorology data. Solar collector field and component capacities are explored and overall performance of the system is evaluated.

In many concentrated solar power systems, power block is operated under fix conditions in order to supply a stable energy output. In SEGS, there is an auxiliary natural gas combustion system which enable the plant to produce constant energy along 24 hours [4]. In utility scale this is requirement is inevitable and preferred by majority of the CSP plants. However in small scale systems and off-grid applications, constant work output is not a must.

In literature there are various published studies about CSP-ORC simulations. Up to my knowledge, majority of the CSP simulations are made with ORC models with constant parameters and flow rate. Power-block operation strategy is either shut-on/shut-off approach [8, 14] or continuous operation with fuel back-up. When irradiation is not sufficient an auxiliary heater is taken into account [11]. In this thesis, different operation parameters of both ORC and CSP system are explored in order to maintain a continuous work output without implementing any auxiliary heater.

The aim is of this study is to maximize work output of a small-scale solar ORC system using optimum design parameters during annual operation.

3. BACKGROUND

3.1. Parabolic Trough Geometry

A Parabolic Trough collector system is constituted by these following parts:

- A parabola shaped reflector surface
- Absorber Pipe in the focal line along the surface
- Heat Transfer fluid (HTF) circulating inside the pipe.

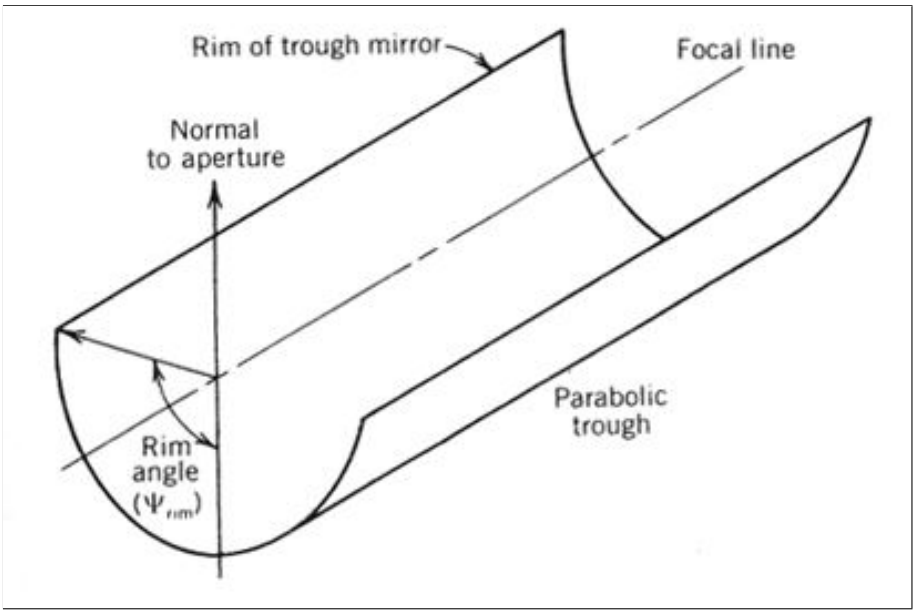

Figure 3.1. Collector Geometry [15].

The parabolic shaped mirrors reflects the solar radiation on the absorber tube. The tube passes through the focal line of the parabola. Inside the tube, heat transfer fluid (HTF) circulates and gains energy to transfer it to a power cycle. The cross section of the parabolic trough is shown in Figure 3.2. The parabolic shaped surface may be either glass or film coated metal sheet. The curve of mirror cross section can be expressed as:

$$y^2 = 4fx \tag{3.1}$$

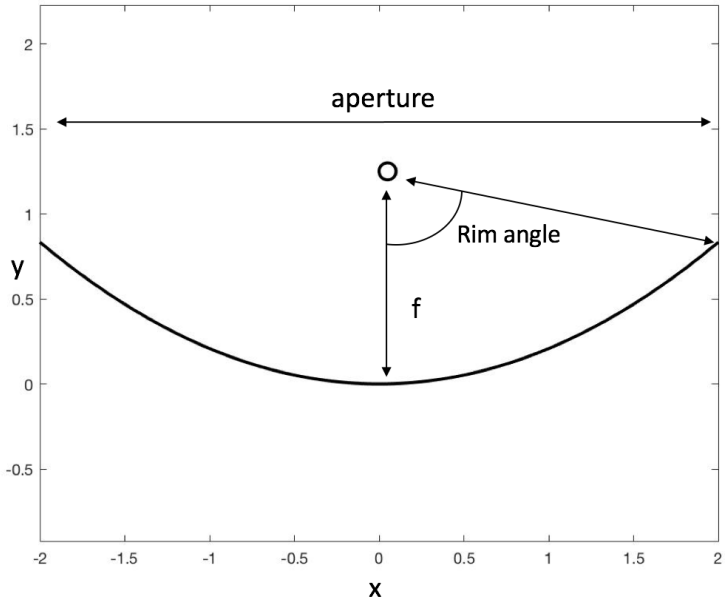

Figure 3.2. Collector cross-section.

where f is the focal distance from the most bottom part of the parabola and a is the aperture width of the shape. The rim angle ϕ_r is defined as [16]:

$$\phi_r = tan^{-1}\Big(\frac{8(f/a)}{16(f/a)^2 - 1}\Big) \tag{3.2}$$

The relation between the focus length and the aperture width determines the curvature of the surface. Using Monte Carlo Ray Tracing Method, Ya-Ling He *et al.* [17] found that after 15°, the rim angle variation does not significantly effect the heat output of the collector surface. Due to practical reasons, commercial parabolic troughs have rim angle around 80° [18].

The geometric concentration ratio is the ratio between the collector aperture area and the total absorber tube area. This ratio varies from 1:1 to 70:1. The formula for the concentration ratio is:

$$C_g = \frac{Wl}{\pi d_0 l} \tag{3.3}$$

where d_0 is the outer diameter of the pipe, l is collector length and W is the aperture width. Receiver or Heat Collecting Element is a glass covered tube designed to reduce

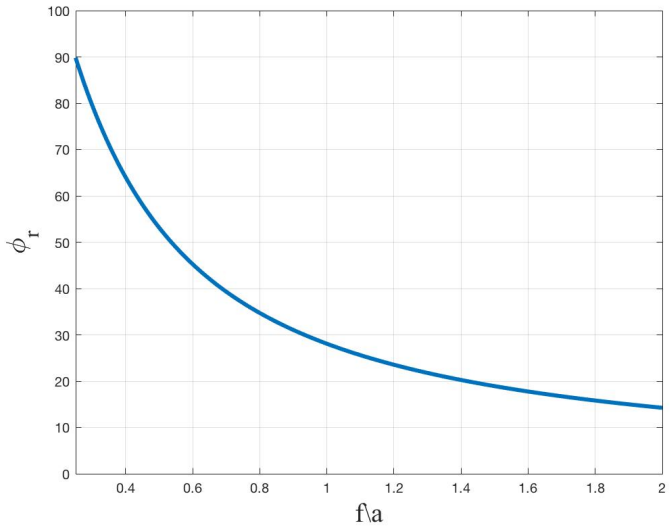

Figure 3.3. Rim Angle for the Collector.

heat transfer losses and increase absorption of the solar radiation. The annulus between tube and the glass is evacuated generally to reduce convection heat transfer. The diameter of the receiver tube is a function of the mirror surface geometry. The focal zone of the collector changes with the rim angle. To maximize the interception of all solar rays, the diameter of the receiver is expressed as [16]:

$$D = \frac{asin(0.267)}{sin\phi_r} \tag{3.4}$$

3.2. Thermal Storage Systems for CSP

Discontinuities and fluctuations in energy supply is one of the major concerns of a solar power system. This problem can be handled by implementing a Thermal Energy Storage (TES), which keeps the solar energy in its heat form. Thermal storage for concentrated solar power plants offers to supply electricity needed without any fossil fuel backup. Also if it is connected to grid, the plant can provide energy especially in peak times of electricity usage during evening hours in residential area. Practically, TES systems can be divided into three categories, sensible heat storage, latent heat storage and chemical storage.

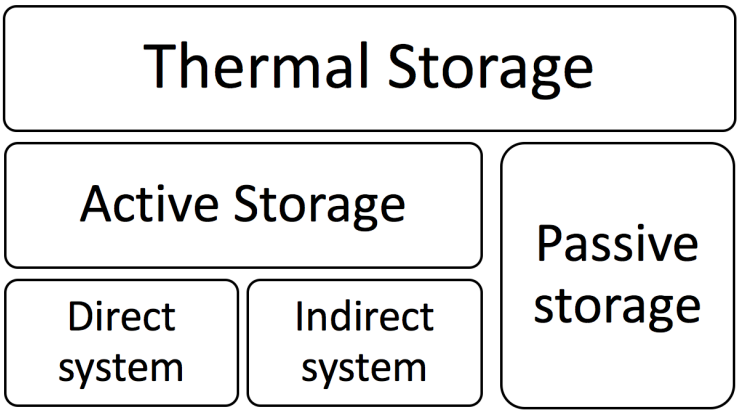

Figure 3.4. Classification of storage systems.

Sensible storage systems basically rely upon storing the energy by heating a media which is well insulated. When the temperature of an object is increased, the amount of the energy that is carried also increases. This energy can be used when it is needed by allowing the cool down of the material in a controlled manner. Sensible heat storage systems is the most used system in commercial plants.

Energy storage capacity of a material is directly related to its specific heat energy and the efficiency of the system decreases with elevation of the temperature. Latent heat storage methods are based on high specific latent energy of the materials. Phase change of a material can store or release a great amount of energy without a significant change in the temperature.

Chemical storage technology is based on reversible endothermic chemical reactions. The heat can be stored by breaking the bonds of the molecules and harvested by allowing them to synthesis again.

All three storage mechanism can be applied with various materials according to desired storage temperature and duration. With respect to thermal storage methods for solar power, plants can be separated as active or passive systems [19].

3.2.1. Sensible Heat Storage

Sensible heat storage is storing energy by heating the material without any phase change during temperature change. The energy stored in the material can be expressed as:

$$Q = \int_{T_i}^{T_f} \rho V c_p(T) dT \tag{3.5}$$

The heat storage capacity of the material is directly connected to density and specific heat, therefore compact materials with high c_p are naturally good candidates as sensible storage medium. Conductivity is also important parameter for energy losses and diffusivity is an important parameter for the time of charge-discharge process.

Storage materials may be solid or liquid. Among solids, concrete and ceramics are most used materials in packed bed form. Main advantages of the solid storage materials are low risk of leakage and resistance to higher temperatures. Solid materials can be coupled with a fluid such as air or oil. In this case TES system can be called as dual system [20].

Most used liquid materials for sensible heat storage are mineral oils, synthetic oils and salt compounds. Liquid storage materials maintain a distinctive temperature gradient vertically due to density change due to temperature. This enables to supply cold fluid from bottom part and extract high temperature from the top. Another advantage of the liquid materials is that they can be used as both HTF and TES media. Molten salts are preferred in solar tower system due to their efficiency and low cost. However the freezing point of molten salt is very high. HitecXL, a commercial salt product for solar towers, which is a mixture of 60% $NaNO_3$ and 40% KNO_3 has a melting point of 220 °C [19]. Therefore an auxiliary heating is necessary to keep salt mixture in fluid phase during nights and low insolation periods. The major disadvantage of the oils is their degradation temperature is lower then molten salts which make them infeasible in solar tower plants [21].

Traditionally, two tank thermal storage systems are developed and tested for CSP plants.. The SEGS I plant had a two tank thermal storage system which used an heat transfer oil, Caloria as storage medium. To reduce cost for the storage systems for this plant, single tank thermocline systems are proposed by Pacheco *et al.* [22].A similar study is conducted by Kolb *et al.* [23] for Saguaro, 1 MW CSP-ORC plant in Arizona.

In a thermocline heat storage system, HTF with high temperature coming from a solar field is charged into a tank from the upper part, which forces the cold fluid in the lower part of the tank to return to the solar field. When collector output temperature is not enough to operate the power cycle, the hot HTF stored at the upper part of the tank is discharged and goes to power block to evaporate the working fluid and returns to the bottom of the tank as a cold fluid. Due to density change with respect to temperature, a distinctive temperature gradient is formed vertically. Using stratification, the heat transfer due to convection of the fluid is minimized [16].

3.2.2. Latent Heat storage

Thermal energy can be stored by as a latent heat of the phase change (solid-liquid or liquid-vapor). Since phase change absorbes a significant amount of heat in without any significant temperature increase, the phase change materials (PCM) are subject of various studies.

Latent Heat Storage systems conserve the energy in phase change of the storage substance. Since the temperature remains same during phase change operation, this type of systems can keep more energy relatively low temperatures therefore total heat losses is reduced. The material suitable for this type of process are called Phase Change Materials (PCM).

PCM systems have advantage in performance and sizing however their implementation requires much more attention and degradation is reported after a certain number of phase change cycles [19].

3.2.3. Chemical Energy storage

Using reversible endothermic reactions for energy storage is another interest of research. Main advantage of this technology is higher storage potential and theoretically infinitely long storage time however this type of systems are under development and not commercially available. Among chemical storage materials, Ammonia is one of the most studied material. The storage concept of liquid ammonia can be expressed by the reactions [24].

$$\begin{aligned} 2NH_3 + heat &\rightarrow N_2 + 3H_2 \\ N_2 + 3H_2 &\rightarrow 2NH_3 + heat \end{aligned} \tag{3.6}$$

3.3. Fluid Selection for Organic Rankine Cycles

The working fluid selection is an important part of the design of an Organic Rankine Cycle because the fluid properties determines the cycle limits and operation condition.

A major parameter to choose the fluids for organic Rankine cycle is the shape of the T-s diagram of the fluid. Working fluids can be classified according to their saturation vapor line in T-s diagrams: "wet" fluids, "dry" fluids and "isentropic" fluids. Wet fluids have a negative slope in their vapor saturation line therefore after expansion in the turbine, the fluids tend to be in the vapor dome which might be harmful for the turbine. To work with this kind of substances, super heating process should be applied in the evaporator. Water is an example of wet fluids. Dry fluids have a positive slope on the T-s curve, therefore an expansion from a saturation point will result that fluid stays in vapor state, therefore these fluids may be operated in their saturation states in the expander inlet. R245fa is an example of a dry fluid. In isentropic fluids, this slope is nearly vertical which is also appropriate for a cycle without super heating. R11 is an example of isentropic fluids. Shape of the T-S diagrams for these fluids are shown in Figure 3.5.

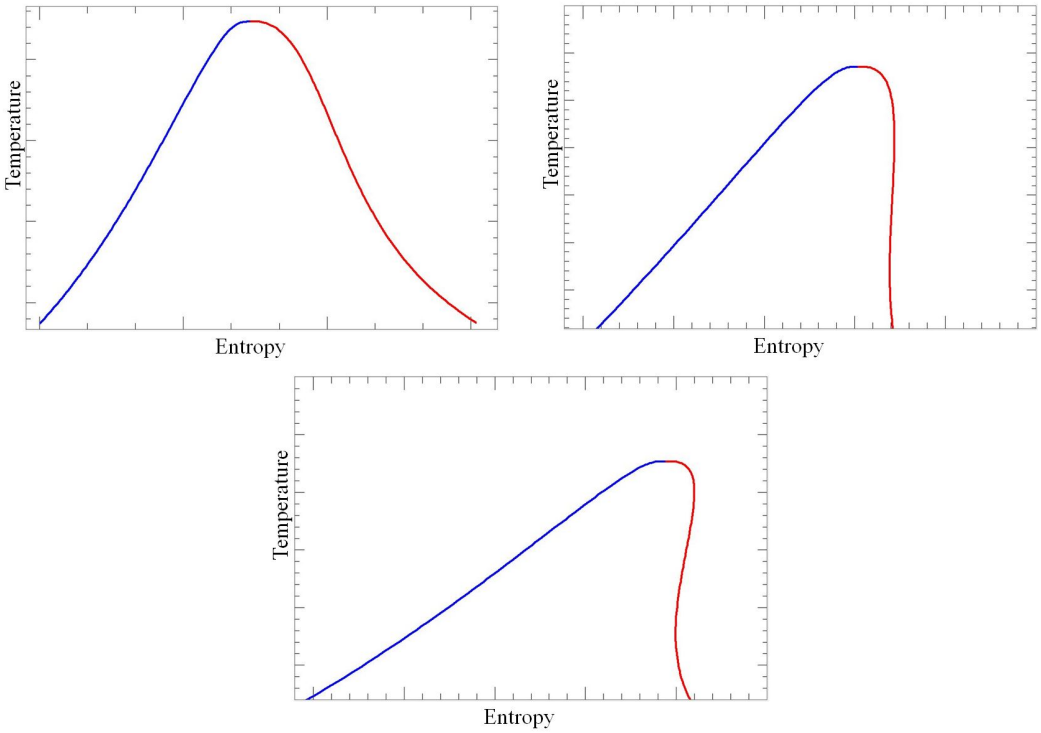

Figure 3.5. T-s diagram for fluids, (a) wet, (b) isentropic, (c) dry.

Another important parameter for working fluid is the evaporation temperature. It simply determines the limits of the system. Temperature of the heat source should be higher then the evaporation temperature of the working fluid in desired pressure. Rayegan *et al.* [25] suggest a selection method applying it in the whole fluid database of the Refprop software. According to this study which is based only on the saturated ORC system, disregarding the superheated ORC systems. Procedure can be outlined in Figure 3.6. According to this study among refrigerants, R245fa and R245ca are the best choices for medium temperature applications (Evaporation temperature=130 °C) and for non-refrigerant fluids butane and isopentane show better performance with respect to other fluids.

Tchanche *et al.* [26] made a similar work for low temperature solar ORC system in which heat source maximum temperature is limited to 90°C. Performance analysis is performed for 20 different working fluids for 2 kW power system. The results show that R134a , R152a and R290 are best selections for low temperature applications. Bao *et al.* [27] made a comprehensive review of working fluids including pure substances as well as the zeotropic fluids. In this study, the expander types of previous fluid selection

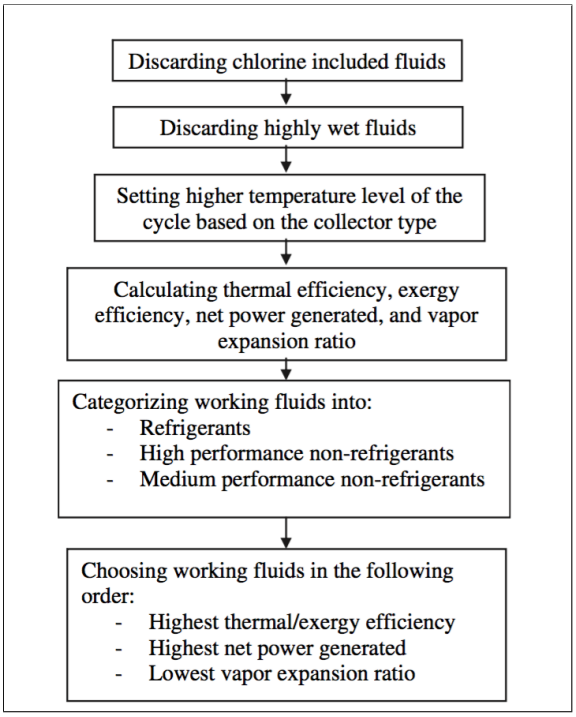

Figure 3.6. Selection procedure of the working fluid in a solar ORC [25].

studies are evaluated. Chen et al. [28] screened 35 fluids for ORC and supercritical ORC system based on their material properties and suggest fluids with low critical temperatures for supercritical systems.

Biomass power plants operate relatively higher temperatures, therefore, the fluids suitable for these systems are totally different than the ones discussed earlier. Drescher *et al.* [29] suggests suitable ORC fluids like OMTS (Octamethyltrisiloxane), Toluene, Ethylbenzene, Propylbenzene and Butylbenzene for biomass ORC plants.

The main idea derived from these studies is that the fluid selection analysis must be done for system specific conditions. Since there is no perfect fluid, there will be always a compromise between several parameters. In order to choose correct simulation, the limiting conditions of the system such as temperature and pressure should be determined and the performance of the preliminary design of the system with suitable fluids should be compared in terms of efficiency and net output energy. Beside, for a given cycle performance, important parameters to consider when choosing a working fluid can be expressed as:

- Evaporation point. The evaporation temperature of the fluid used directly affects the flow rates and efficiency of the system.
- Slope of the saturation vapor curve. The slope of the curve determines whether there is a need for superheating or not, therefore it really effects the efficiency of the system.
- Vapor density. Fluids with low vapor density leads to increase in volume of the heat exchanger, therefore system in generally.
- Low Ozone Depleting Potential. ODP is the degradation level in ozone that may a chemical compound can cause. The ODP levels of compounds scaled with respect to R-11 (Trichlorofluoromethane) which has a ODP value of 1.
- Global Warming Potential (GWP). GWP is the relative measure of how much heat a greenhouse gas traps in atmosphere with respect to carbon dioxide.
- Flammability and Toxicity. ASHRAE standard 34 may be used to determine whether the fluid is in the safe list or not.

Among the extensive studies and reviews about the cycle fluid selection, the fluids in Table 3.1 are the most outlined ones proposed for small scale solar ORC systems.

Table 3.1. Selected ORC fluids for CSP applications.

Substance	Molecular Mass	$T_{critical}$	$P_{critical}$	$T_{evaporation}$	ODP	GWP
R245fa	134.05	154.01	3.64	15.14	0	950
R123	152.93	183.68	3.668	27.82	0.020	77
Isobutane	58.12	134.70	3.63	-11.73	0	20
R134a	102.03	101.06	4.06	-26.07	0	1430

3.4. Radiation Definitions

There are three main terms of radiation which is needed to be defined [2].

- Direct Normal Irradiance (DNI) is the amount of solar radiation received per unit area by a surface that is perpendicular to rays of the Sun. The amount of solar radiation annually received by a surface can be maximized by solar tracking

systems which enables CSP systems to utilize the majority of the DNI component.

- Diffuse Horizontal Irradiance (DHI) is the amount of solar radiation received per unit area by a surface that does not arrive directly from the Sun, but has been scattered by molecules or and particles in the atmosphere or reflected from other bodies from other direction directions.
- Global Horizontal Irradiance (GHI) is the total amount of shortwave radiation received from above by a horizontal surface. This term is the sum of Direct Normal Irradiance (DNI) and Diffuse Horizontal Irradiance (DHI).

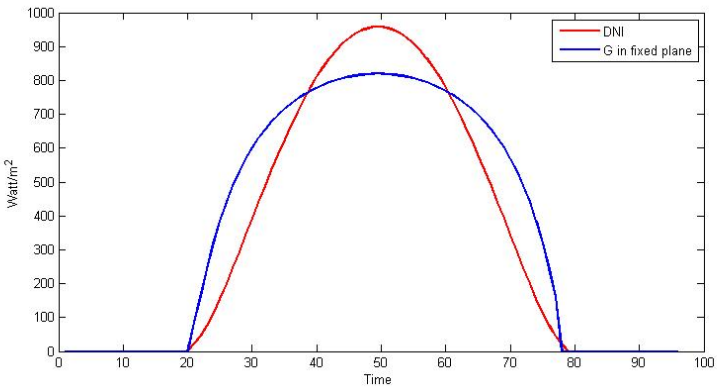

Figure 3.7. DNI vs GHI values for fixed plane for Antalya in June.

4. THERMODYNAMIC MODEL METHODOLOGY

4.1. System Model Description

In this study a regenerative organic Rankine cycle system with thermocline thermal storage system is implemented as in the Figure 4.1. As a heat source, the parabolic trough model is used. All system components are developed in Matlab environment in order to simulate with annual meteorology data of given location.

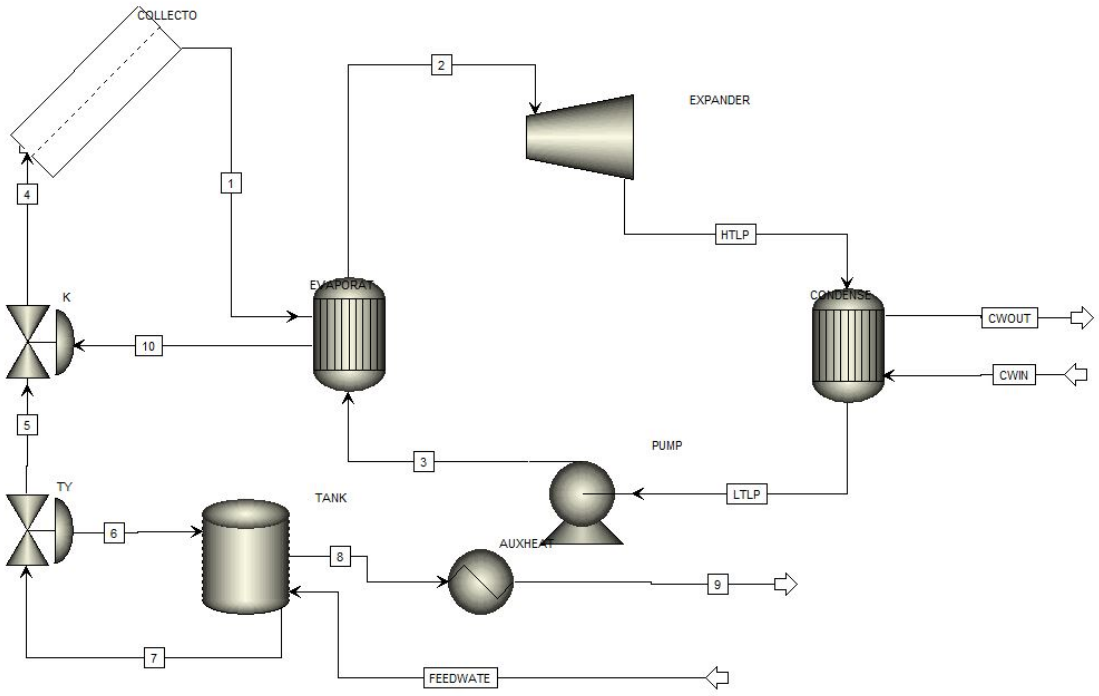

Figure 4.1. Organic Rankine Cycle

The fluid used for the study is R245fa. The states of the cycle and the T-s diagram of the fluid is Figure 4.2.

4.2. Parabolic Collector Model

Using this method the total thermal resistance can be calculated between the heat transfer fluid and ambient therefore total temperature increase in the collector is found.

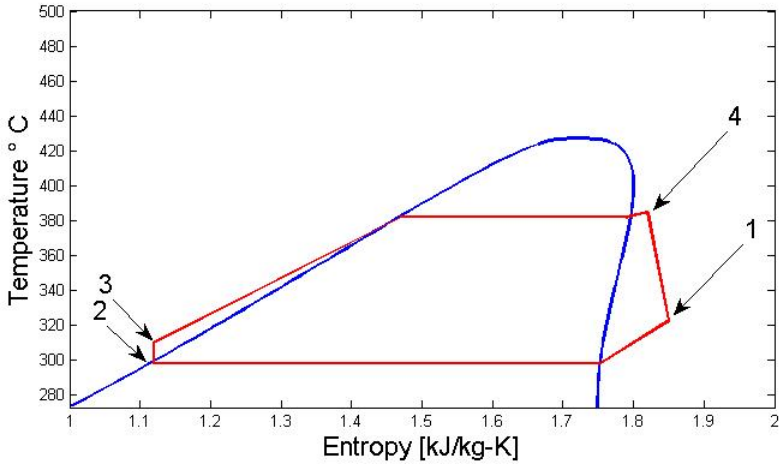

Figure 4.2. T-s Diagram for R254fa

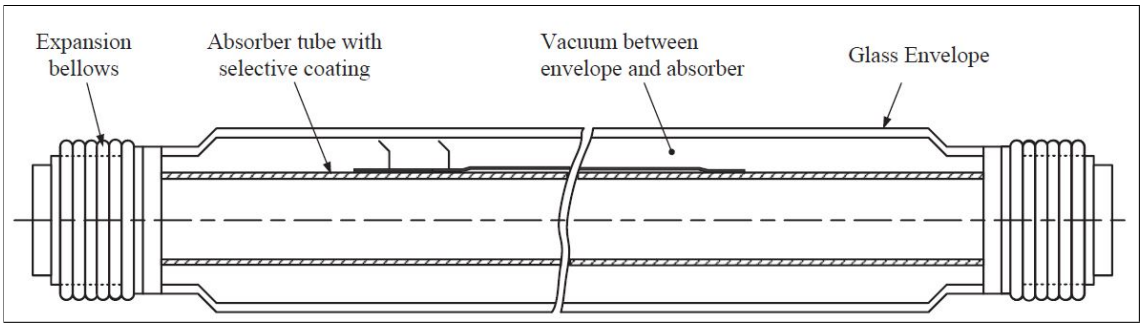

Figure 4.3. Parts of a heat collection element (HCE) and control volume used for the heat transfer analysis. Adapted from [30].

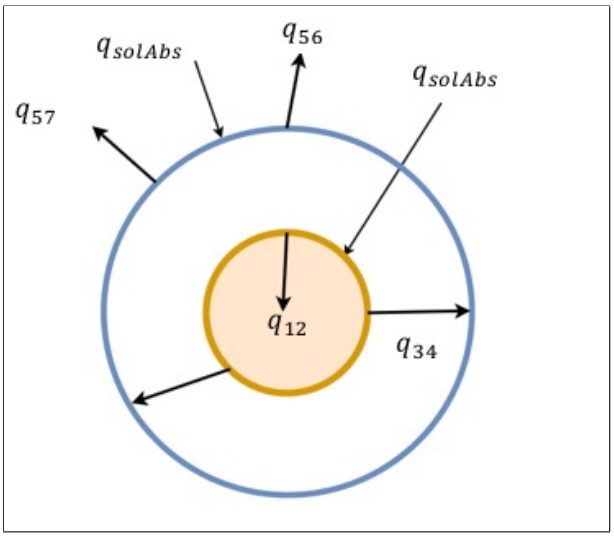

Figure 4.4. Energy Balance in receiver cross section

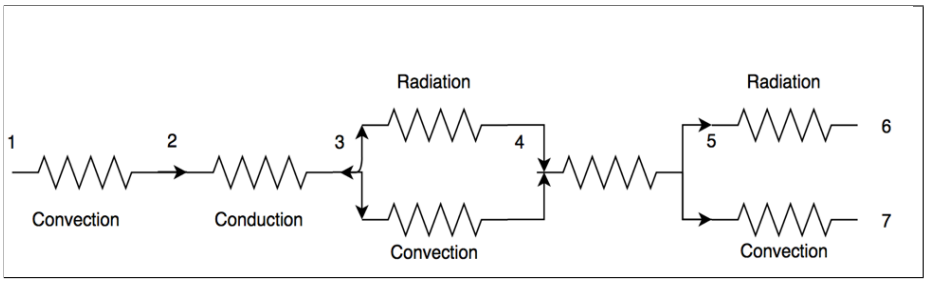

Figure 4.5. Thermal resistance model of the receiver in radial direction

The heating process is considered as quasi-static process where energy is transfered along the radial direction. This thermal resistance model can be summarized in Figure 4.5 where the node 1 is fluid temperature, the node 2 is receiver inside temperature, the node 3 is receiver outside temperature, the node 4 is glass cover inside temperature, the node 5 is glass cover outside temperature, the node 6 is sky temperature and the node 7 is ambient temperature:

Energy balance equations can be written considering heat transfer rates in the cross sectional area:

$$\dot{q}_{12conv} = \dot{q}_{23cond} \tag{4.1a}$$

$$\dot{q}_{3SolAbs} = \dot{q}_{34conv} + \dot{q}_{34rad} + \dot{q}_{23cond} + \dot{q}_{cond,bracket} \tag{4.1b}$$

$$\dot{q}_{34conv} + \dot{q}_{34rad} = \dot{q}_{45cond} \tag{4.1c}$$

$$\dot{q}_{45cond} + \dot{q}_{5SolAbs} = \dot{q}_{56conv} + \dot{q}_{57rad} \tag{4.1d}$$

$$\dot{q}_{HeatLoss} = \dot{q}_{56conv} + \dot{q}_{57rad} + \dot{q}_{cond,bracket} \tag{4.1e}$$

(i) Convection heat transfer between the HTF and the receiver pipe. The heat transfer between HTF and the receiver pipe is modeled as a forced convection. It may be calculated by using Newton's Law of Cooling:

$$\dot{q}_{12conv} = h_1 \pi D_2 (T_2 - T_1) \tag{4.2}$$

Where the fluid temperature is assumed as uniform in the cross-section. Heat transfer coefficient inside the pipe, h_1 can be found by formula below.

$$h_1 = Nu_{D_2}\frac{k_1}{D_2} \tag{4.3}$$

To determine the convective heat transfer coefficient, an appropriate Nusselt number correlation for internal flow should be used. In steady state conditions, flow in the parabolic collector system is expected to be developed and turbulent, however it might be laminar in the transition times therefore correlations for both flow regimes should be considered. To determine Nusselt number in turbulent flow (Re $>$ 2300), the correlation of Gnielinski [31] is used.

$$Nu_D = \frac{(fr_2/8)(Re_{D_2} - 1000)Pr_1}{1 + 12.7\sqrt{fr_2/8}(Pr_1^{2/3} - 1)} \tag{4.4}$$

with friction coefficient fr can be found using [31],

$$fr_2 = (1.82log_{10}(Re_{D_2}) - 1.64)^{-2} \tag{4.5}$$

if flow is laminar then Nusselt number has a constant value for internal pipe flow, Nu=4.364.

(ii) Conduction heat transfer through the receiver pipe wall. Conduction heat transfer in the pipe can be calculated by this formula:

$$\dot{q}_{23,cond} = \frac{2\pi k_{23}(T_2 - T_3)}{\ln(\frac{D_3}{D_2})} \tag{4.6}$$

conductivity of the pipe, k_{23} can be taken as constant or the value of the average temperature of the receiver. This conductivity depends on the material itself. Therefore material of the pipe must be selected before calculating heat flux. For copper, thermal conductivity is equal to 385 W/m-°C. If the receiver pipe is stainless steel there are formulas derived from linear fitting by Davis [32]. If the

pipe is stainless steel 304L or 316L, the conductivity is expressed as:

$$k_{pipe} = (0.013)T_{pipe} + 15.2 \tag{4.7}$$

for steel 321H and

$$k_{pipe} = (0.0153)T_{pipe} + 14.775 \tag{4.8}$$

and for steel 316L.

(iii) Convective heat transfer from the receiver pipe to the glass envelope. Heat transfer between the receiver pipe and the glass envelope has to modes: convection and radiation. The conduction between support connecting these elements can be neglected because of their size.

Convection heat transfer between the receiver and the glass envelope depends on the density of the air or other gases in the annulus. If annulus is in vacuum (P$<$ 0.013 Pa), the convection coefficient is calculated as: [33]

$$h_{34} = \frac{k_{std}}{D_3/2\ln(D_4/D_3) + b\lambda(D_3/D_4 + 1)} \tag{4.9}$$

where k_{std} is the thermal conductance of the annulus gas at standard temperature and pressure and b is interaction coefficient defined by Ratzel et al. [34].

$$b = \frac{(2-a)(9\gamma - 5)}{2a(\gamma + 1)} \tag{4.10}$$

with γ is ratio of specific heats for annulus gas and λ is mean-free path between collisions of a molecule which can be calculated as:

$$\lambda = \frac{(2.331 \times 10^{-20})(T_{34} + 273)}{P_a \delta^2} \tag{4.11}$$

where δ is the molecular diameter of the air, which is assumed as $3.55 \times 10^{-}8$.

Table 4.1. Heat Transfer Coefficients and Constants for Each Annulus Gas [35].

Annulus Gas	k_{std} [W/m-K]	b	λ [cm]	γ	δ [cm]	h_{34} [W/mˆ2-K]
Air	0.02551	1.571	88.67	1.39	3.53E-8	0.0001115
Hydrogen	0.1769	1.581	191.8	1.398	2.4E-8	0.0003551
Argon	0.01777	1.886	76.51	1.677	3.8E-8	0.00007499

This model is valid for:

$$Ra_{D_4} < (D_4/(D_4 - D_3))^4 \tag{4.12}$$

The tabulated data for several gas is given by Forristall [35] in Figure 4.1.
If there is pressure in the annulus, the convection between to material is explained with natural convection. One of the formulas from the literature may be used for concentric cylinders:

$$\dot{q}_{34conv} = \frac{2.425 k_{34}(T_3 - T_4)(PrRa_{D3}/(0.861 + Pr_{34}))^{1/4}}{\left(1 + (D_3/D_4)^{3/5}\right)^{5/4}} \tag{4.13}$$

with Rayleigh number is expressed as:

$$Ra_{D3} = \frac{g\beta(T_3 - T_4)D_3^3}{\alpha\nu} \tag{4.14}$$

with β is equal to volumetric thermal expansion coefficient (1/K), ν is kinematic viscosity, α is thermal diffusivity and g is gravitational acceleration. For ideal gases, β is equal to:

$$\beta = \frac{1}{T_{avg}} \tag{4.15}$$

(iv) Radiation Heat Transfer between receiver pipe and glass envelope To calculate the radiative heat transfer, some assumptions are made for the sake of simplicity:

- no participating gas in the annulus.

- all surfaces are gray
- no participating gas in the annulus
- glass envelope is opaque to infrared radiation

then the heat transfer can be calculated as follows:

$$\dot{q}_{34,rad} = \frac{\sigma\pi D_3(T_3^4 - T_4^4)}{\left(\frac{1}{\epsilon_3} + \left(\frac{(1-\epsilon)D_3}{\epsilon_4 D_4}\right)\right)} \tag{4.16}$$

(v) Conduction heat transfer through the glass envelope Conduction heat transfer in the pipe can be calculated by this formula:

$$q_{45,cond} = \frac{2\pi k_{45}(T_4 - T_5)}{\ln(\frac{D_5}{D_4})} \tag{4.17}$$

For Pyrex glass, thermal conductivity is equal to 1.04 W/m-°C.

(vi) Heat transfer from the glass envelope to the atmosphere Convection between the envelope and the atmosphere may be explained by convection where:

$$q_{56,conv} = h_{air}\pi D_5(T_5 - T_6) \tag{4.18}$$

Heat transfer coefficient h_{air} can be found by this correlation.

$$h_{air} = Nu_{D_5}\frac{k_{air}}{D_5} \tag{4.19}$$

Considering the estimated wind speed, among different correlations, Zhukauskas's correlation is selected [31]:

$$Nu_D = CRe_{D_5}^m Pr_6^n(\frac{Pr_6}{Pr_5})^{\frac{1}{4}} \tag{4.20}$$

This correlation is valid for cross flows around a cylinder for $1 < Re_{D_5} < 10^6$ and $0.7 < Pr < 500$. The constants are given in Table 4.2.

(vii) Radiation Heat Transfer Net heat transfer between cover itself and the environ-

Table 4.2. Zhukauskas correlation coefficients.

Re	C	m
$1-40$	0.75	0.4
$40-1000$	0.51	0.5
10^3-2 x 10^5	0.26	0.6
$2\text{x}10^5-10^6$	0.076	0.7

Table 4.3. Optical Efficiency Terms provided by Forristall [35].

ϵ_{sh}	Receiver shadowing (bellows, shielding, supports)	0.974
ϵ_{tr}	Tracking error	0.994
ϵ_{ge}	Geometry error (mirror alignment)	0.98
ρ_{cl}	Clean mirror reflectance	0.935
ϵ_{dm}	Dirt on mirrors	(ρ/ρ_{cl})
ϵ_{dr}	Dirt on receiver	$(1+\epsilon_{dm})/2$
ϵ_{un}	Unaccounted	0.96

ment through radiation is expressed as:

$$\dot{q}_{5-7,rad} = \sigma\epsilon_5\pi D_5(T_5^4 - T_7^4) \tag{4.21}$$

(viii) Solar irradiance absorption Solar radiation absorbed by the glass cover is

$$q_{5,SolAbs} = q_{sol}\eta_{env}\alpha_{env} \tag{4.22}$$

where η_{env} is effective optical efficiency of the cover and α is absorptivity of the glass cover. Optical efficiency of the glass is:

$$\eta_{env} = \epsilon_{sh}\epsilon_{tr}\epsilon_{ge}\epsilon_{dm}\epsilon_{dr}\epsilon_{un}\rho_{cl}K_\theta \tag{4.23}$$

These coefficients are provided by Forristall [35] in Table 4.3. Single axis tracking systems get the radiation with a certain incidence angle, therefore there should

be a correction factor, experimental results from Sandia Lab [36] shows that:

$$K_\theta = cos(\theta) + 0.000804\theta - 0.00005369\theta^2 \tag{4.24}$$

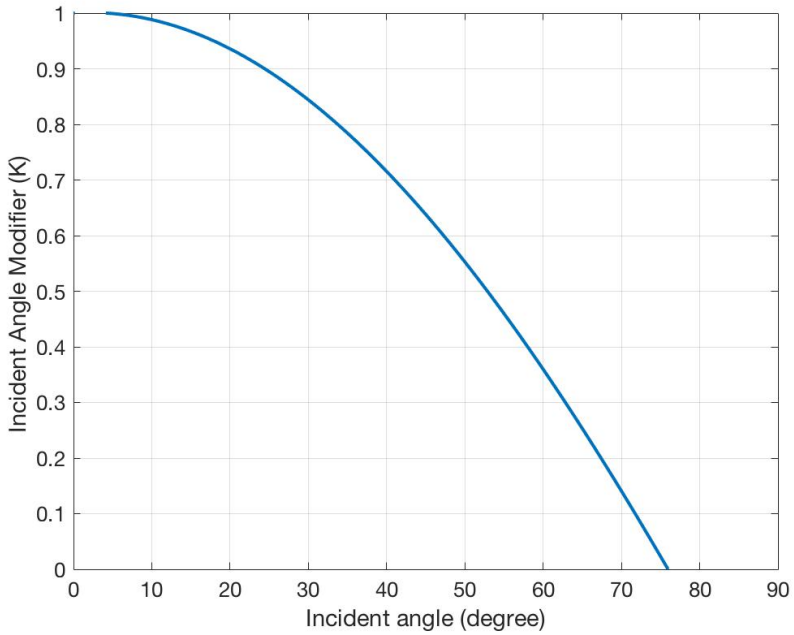

Figure 4.6. Incident angle modifier for LS-2 collector .

Solar irradiation absorption in the receiver is expressed as:

$$q_{5,SolAbs} = q_{sol}\eta_{abs}\alpha_{abs} \tag{4.25}$$

with

$$\eta_{abs} = \tau_{env}\eta_{env} \tag{4.26}$$

4.2.1. Solution method for Thermal Resistance Model

Thermal resistance model have multiple equations to be solved together therefore an iterative scheme should be used as described in Figure 4.7. Solution starts with an initial guess for receiver and glass cover temperature. Total loss from the glass cover

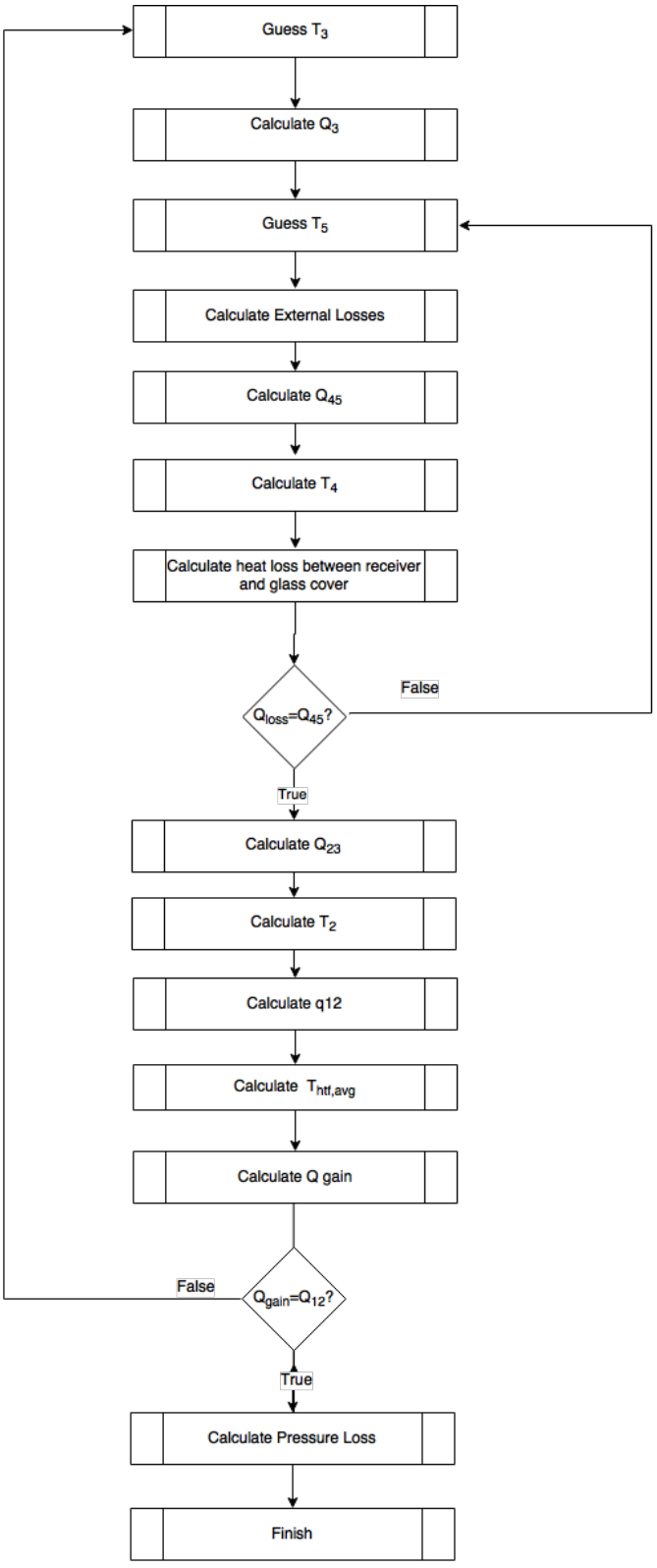

Figure 4.7. Solution method for Solving Thermal Resistance Method.

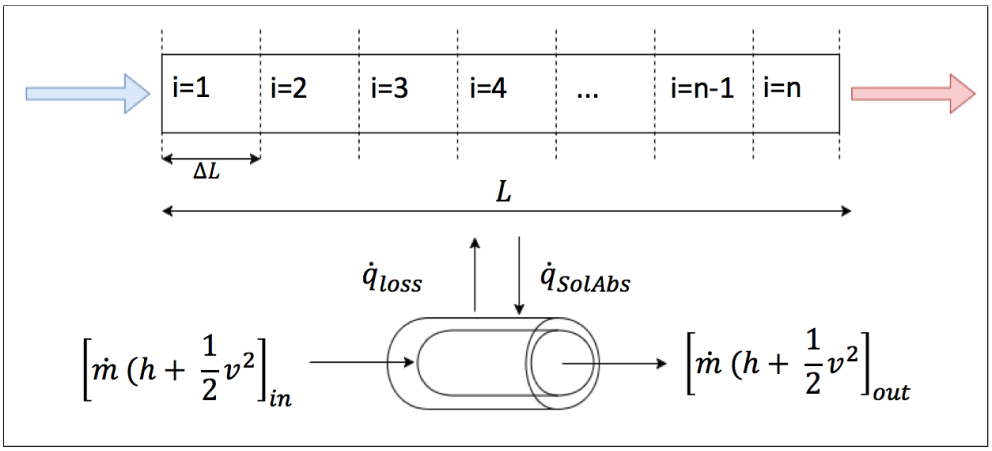

Figure 4.8. Calculation of collector outlet temperature.

surface is calculated using Equation 4.21 and 4.18. Using Equation 4.1e, the inside temperature of the cover is found. Using the energy balance around the glass cover, the temperature is updated for the given receiver outside temperature. Then energy balance is written with respect to receiver surface. This operation is repeated for each finite volume section as shown in Figure 4.8.

4.2.2. Model Validation

To validate the parabolic collector model, test results from the Sandia Lab is used [37]. In this study, a module of SEGS LS-2 type solar collector is tested with two different receiver components several configurations (vacuum in annulus, pressure in annulus and without glass cover) in order to evaluate efficiency curve of the collector and the percentages of the thermal losses. For cermet surface with vacuum annulus case, test results and model results are given in Figure 4.12:

Output values of the model is similar to test data and stay in an acceptable range. Results shows that collector model can be used for further analysis.

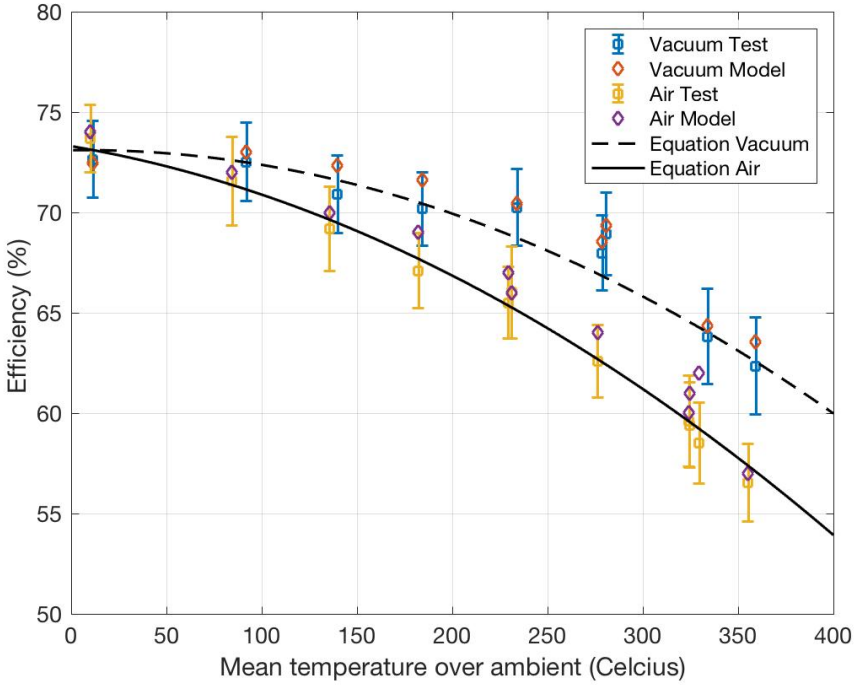

Figure 4.9. Efficiency of cermet receiver with vacuum annulus.

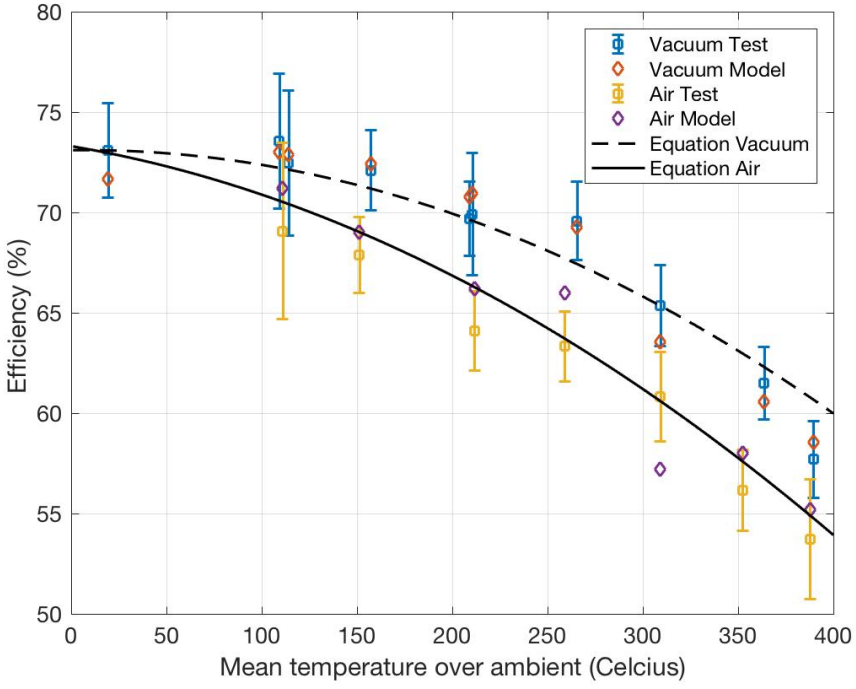

Figure 4.10. Thermal loss of cermet receiver with vacuum annulus.

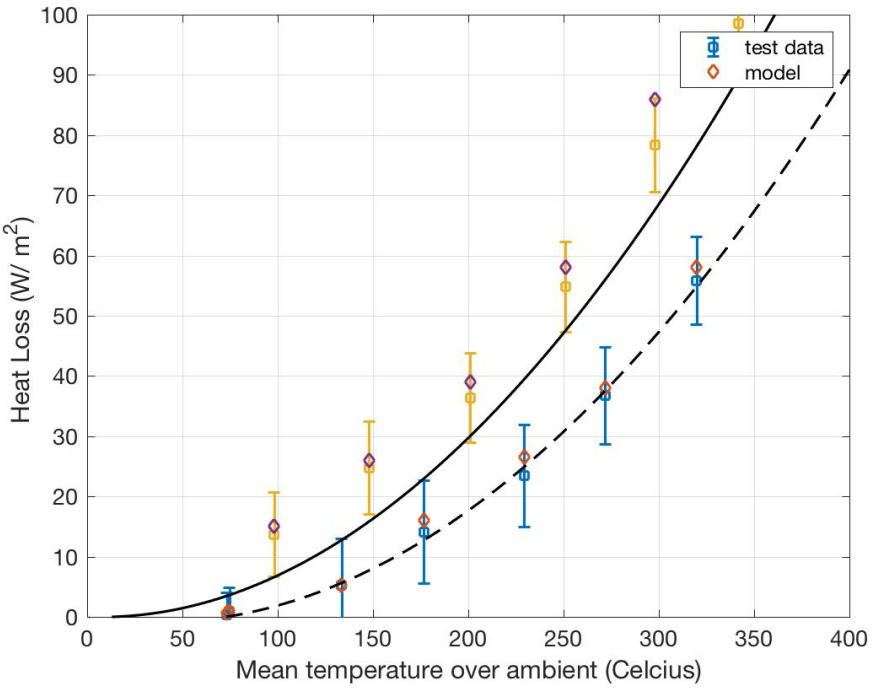

Figure 4.11. Efficiency of cermet receiver with air annulus.

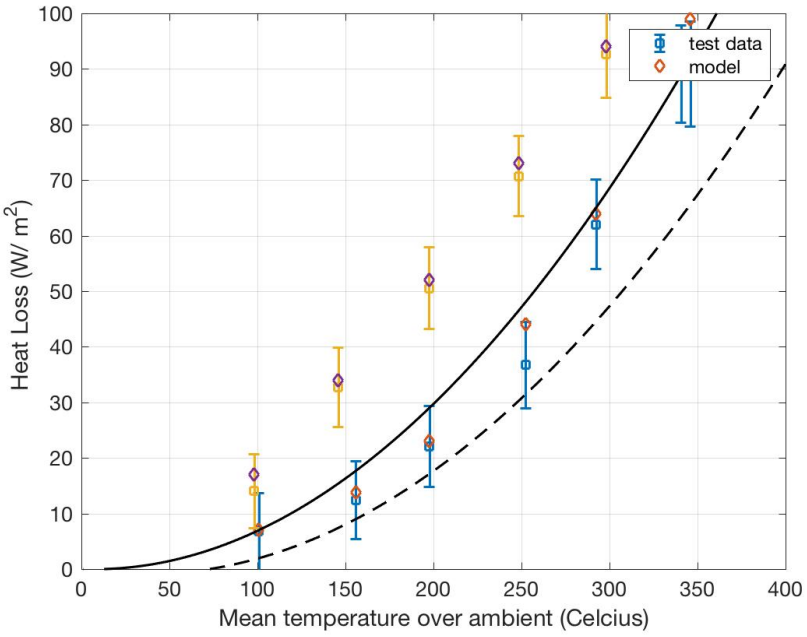

Figure 4.12. Thermal Loss of cermet receiver with vacuum annulus.

Table 4.4. SEGS LS-2 Parabolic Trough Solar Collector Test Specifications [36]

Operating temperature	100-400°C
Module size	7.8 m × 5 m
Rim angle	70°C
Reflectors	Low iron glass with reflectivity: 0.93
Aperture area	39.2 m^2
Focal length	1.84 m
Concentration ratio	71
Absorber diameter	70 mm
Absorber length	4m (x2)
Pyrex glass envelope diameter	115 mm
Pyrex glass envelope transmittance	0.95
Cermet surface absortance	0.96
Cermet surface emittance @350°C	0.14
Black chrome surface absortance	0.96
Black chrome surface emittance @350°C	0.24
Heat Transfer Fluid	Slytherm 800

4.3. ORC system model

Organic Rankine Cycle system is modeled with 4 main components: A pump, an evaporator, an expander and a condenser. As working fluid, R245fa is selected.

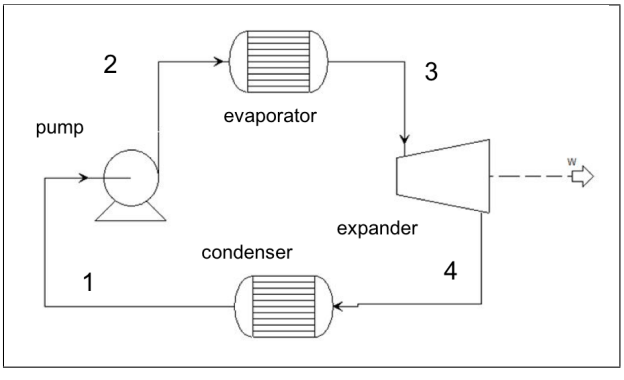

Figure 4.13. ORC cycle diagram.

4.3.1. ORC fluid Pump

The work input required to pressurize the fluid to the evaporation pressure can be calculated using this formula:

$$W_{pump,orc} = \dot{m}_{wf}(h_2 - h_1)/\eta_{combined} \tag{4.27}$$

$\eta_{combined,orc} = 0.90$ is chosen as combined pump efficiency (mechanical and electrical) To calculate enthalpy of pump outlet, the isentropic efficiency formula of the pump with constant $\eta_{pump,orc} = 0.65$ is used below:

$$\eta_{pump,orc} = \frac{h_{2s} - h_1}{h_2 - h_1} \tag{4.28}$$

4.3.2. Evaporator

The heating process of the evaporator is assumed as isobaric (no pressure loss across the evaporator) therefore state 2 and 3 has same pressure. A fixed pinch temperature of $\Delta T_{pinch} = 5$ is assumed in the model. Evaporation process can also include superheating of the fluid in certain conditions. Therefore state 3 temperature of the working fluid at the inlet of the expander is calculated as this formula:

$$T_3 = T_{htf,in} - \Delta T_{pinch} \tag{4.29}$$

As a control check, the pinch temperature difference must be conserved along the evaporator, especially in the beginning of evaporation state of the working fluid. Therefore this condition must be correct for a smooth operation.

$$T_{htf,x} - T_{evaporation} >= \Delta T_{pinch} \tag{4.30}$$

The enthalpy difference of the working fluid in its gas state is :

$$\Delta h_{evaporation-3} = h_3 - h_{boiling} \tag{4.31}$$

so by using this enthalpy balance, the HTF temperature at the boiling process can be found by:

$$T_{htf,x} = T_{htf,in} - \frac{\dot{m}_{htf}\Delta h_{evapotation-3}}{\dot{m}_{htf}c_{p,htf}} \tag{4.32}$$

4.3.3. Expander

Expander isentropic efficiency is expressed by this formula:

$$\eta_{expander,orc} = \frac{h_3 - h_4}{h_3 - h_{4s}} \tag{4.33}$$

$\eta_{expander,orc} = 0.75$ is chosen as isentropic expander efficiency. The power output of the expander can be calculated by the formula:

$$W_{pump,orc} = \dot{m}_{wf}(h_2 - h_1)/\eta_{combined} \tag{4.34}$$

where $\eta_{combined} = 0.90$ is assumed as combined efficiency (electrical and mechanical)

4.3.4. Condenser

For the condenser model, a fixed pinch temperature is assigned between cold stream (air or tap water) and the condensing temperature. The formulation is same as the evaporator model.

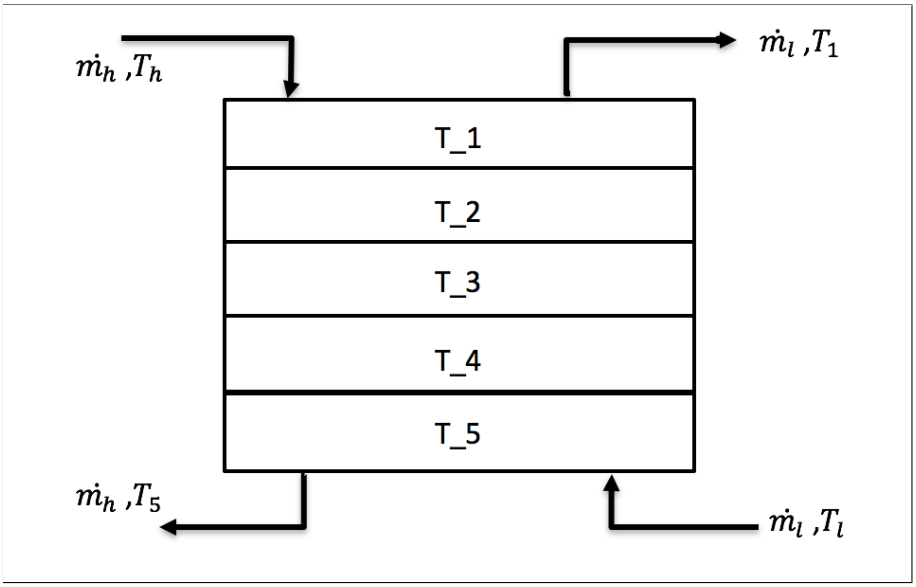

Figure 4.14. Thermocline Storage Tank Model.

4.4. Single Tank Thermal Storage Model

In this study, a single tank storage system is modeled as a sensible heat storage method as shown in Figure 4.14. The similar approach is used by [10], [9] and [8] for small scale CSP applications. To simplify the model, it is assumed that the heat transfer fluid and the fluid inside the tank is fully mixed. Heat loss coefficient of the tank is considered as constant however the ambient temperature varies with the time as irradiation does.

To calculate the temperature distribution in the tank, a multi node approach is used. Tank is divided n vertically placed equal volume and for each volume energy balance is written. For i_{th} layer in the tank the conservation of energy yields [10]:

$$\begin{aligned} m_{f,i}c_{pf,i}\frac{dT_{f,i}}{dt} =& a_i\dot{m}_{f,h}c_{pf,i}(T_{f,h}-T_{f,i}) + b_i\dot{m}_{f,l}c_{pf,i}(T_{f,l}-T_{f,i}) \\ &+ U_{s-env}A_{s,i}(T_{f,i}-T_{env}) + \begin{cases} c_i(T_{i-1}-T_i)c_{pf,i} & c_i > 0 \\ c_i(T_i-T_{i-1})c_{pf,i} & c_i < 0 \end{cases} \end{aligned} \tag{4.35}$$

where for a:

$$a_i = \begin{cases} 1 & i = S_n \\ 0 & i \neq S_n \end{cases} \tag{4.36}$$

for b:

$$b_i = \begin{cases} 1 & i = S_l \\ 0 & i \neq S_l \end{cases} \tag{4.37}$$

and for c:

$$c_i = \dot{m}_{f,h} \sum_{j=1}^{j-1} a_j - \dot{m}_{f,l} \sum_{j=i+1}^{n} b_j \tag{4.38}$$

The losses from the tank is:

$$\dot{Q}_{loss,s} = \sum_{i=1}^{n} U_{s-env}(T_{f,i} - T_{env}) \tag{4.39}$$

and the heat transfered from the collector system to the tank can be expressed as:

$$\dot{Q}_{stored} = \dot{m} \frac{\sum_{i=1}^{n} c_{p,f}}{n} \sum_{i=1}^{n} U_{s-env}(T_{f,i} - T_{env}) \tag{4.40}$$

The energy balance equations for each layer can be solved simultaneously using a Runge-Kutta scheme [16]. For this purpose, a built-in function ODE45 is used in Matlab. The temperature distribution of different layers with a constant mass flow rate in 350 °C from the load side as given in Figure 4.15. Thermal storage tank shape is designed as cylindrical. To determine its heat transfer surface with environment, the dimensions of the tank is parametrized according to its volume the relation between

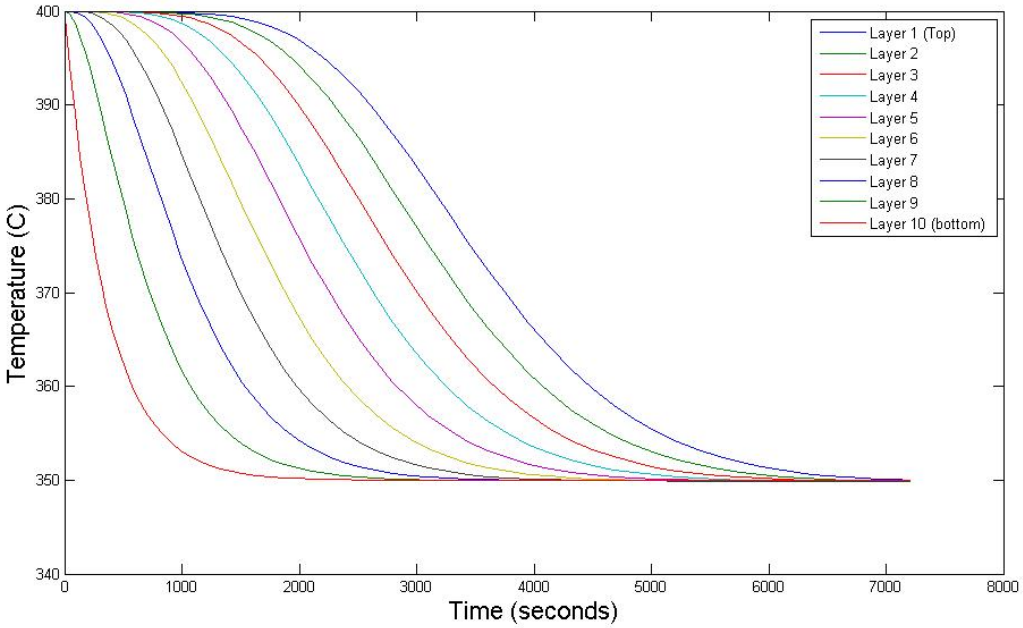

Figure 4.15. Temperature distribution in different layers of the tank.

height (H) and diameter (D) of the cylinder is selected as:

$$H = 4D \tag{4.41}$$

heat loss coefficient of the storage tank is depends on the tank temperature and the insulation type. Using generalized heat coefficient numbers from Table 4.5, heat generation coefficient for the storage model is extrapolated for sheltered and insulated tank loss coefficient values [38]:

4.5. Daily Simulation

To better estimate the capacity of a solar power plant, it is essential to have accurate meteorological data of the location of interest. Generally the most important ambient factors for a solar thermal power system are can be expressed as:

- Radiation (either DNI or GHI)
- Ambient Temperature
- Wind Speed and Direction.

Table 4.5. Heat Transfer coefficients for a standard oil storage tank

Tank position	ΔT between storage medium and ambient	Overall heat transfer coefficient (W/m^2 ° C)	
		Uninsulated	Insulated
Sheltered	Around 10 ° C	6.8	1.7
	Around 27 ° C	7.4	1.8
	Around 38 ° C	8.0	2.0
Exposed	Around 10 ° C	8.0	2.0
	Around 10 ° C	8.5	2.1
	Around 10 ° C	9.1	2.3
Underground	Any Temperature	6.8	-

To make an annual performance evaluation of the system, PVGIS Database is used as a source for radiation and ambient temperature. Photovoltaic Geographical Information System (PVGIS) provides the values for all solar radiation components for to give energy generation potential for given location in Europe, Africa, and South-West Asia [39]. In In the daily radiation dataset, irradiation information is provided for every 15 minutes. Assuming a proper solar tracking system in one axis, the available energy, DNI component of the solar irradiation. Bogazici University Kilyos Kampus location is selected (41.245N, 29.014E) as plant location.

Air and tap water temperatures of Istanbul are provided by Meteoroloji Genel Müdürlüğü website [40]. This information is used to determine condenser cooling water temperature. For "average day" of each month, simulation is made starting from the ambient conditions for both CSP and ORC system. As irradiation increases with time and temperature of the heat transfer fluid passes design set point, it starts to transfer energy to working fluid through the evaporator. If returning heat transfer fluid temperature is higher then the set point temperature, it goes to storage tank for the "charging" process, then return to solar field. When irradiation is become insufficient to heat the fluid up to desired temperature, the tank itself provide necessary thermal

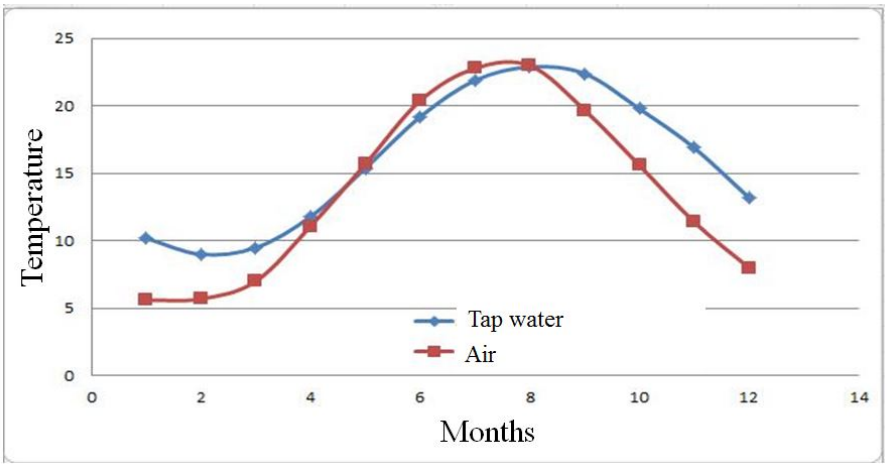

Figure 4.16. Monthly water and air temperatures of Istanbul.

output for a while. System efficiency for the simulations are defined as:

$$\text{System efficiency} = \frac{\text{Daily work output}}{\text{Daily solar irradiation}} \tag{4.42}$$

5. RESULTS AND DISCUSSION

For annual simulation, a base design for ORC is selected with the specifications in Table 5.1.

Table 5.1. Base ORC specifications for simulation.

Working Fluid	R245fa
Evaporation Temperature	101 °C
Condensation Temperature	25 °C
WF Mass flow rate	0.3 kg/s
Pressure ratio	10.8
Net power output	9.53 kW
Cycle efficiency	0.12
HTF mass flow rate	1 kg/s

Minimum pinch temperature for evaporator is set to 5 °C. Therefore minimum required temperature at collector outlet is set to 407 °K. This temperature is called as "set temperature" for orc system activation and is shown in the figures by red line. Annual simulation results for Istanbul with a collector field of 200 m^2 is shown from Figure 5.1 to 5.12.

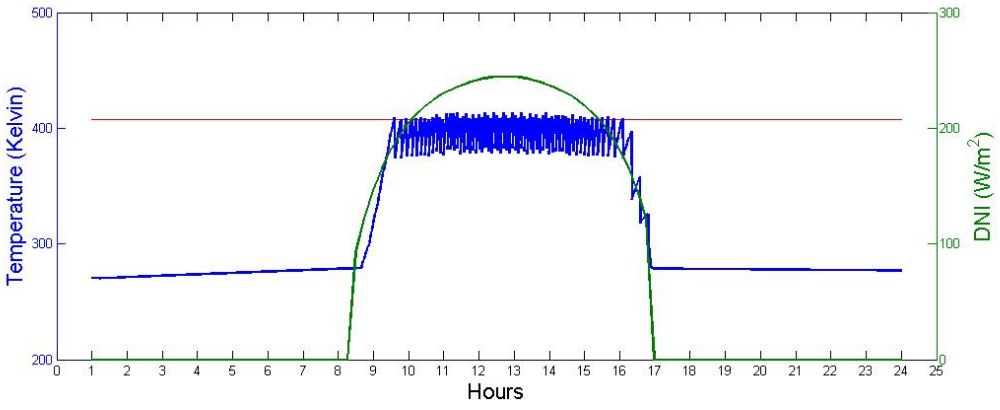

Figure 5.1. Daily irradiation and collector output temperature in January.

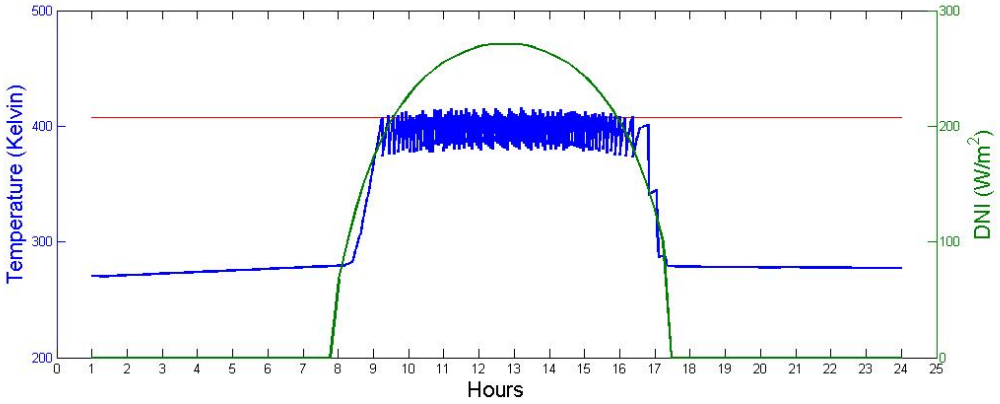

Figure 5.2. Daily irradiation and collector output temperature in February.

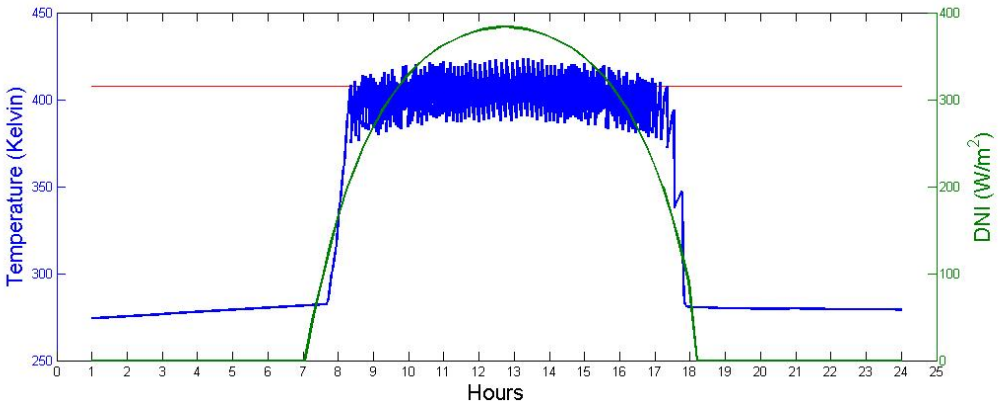

Figure 5.3. Daily irradiation and collector output temperature in March.

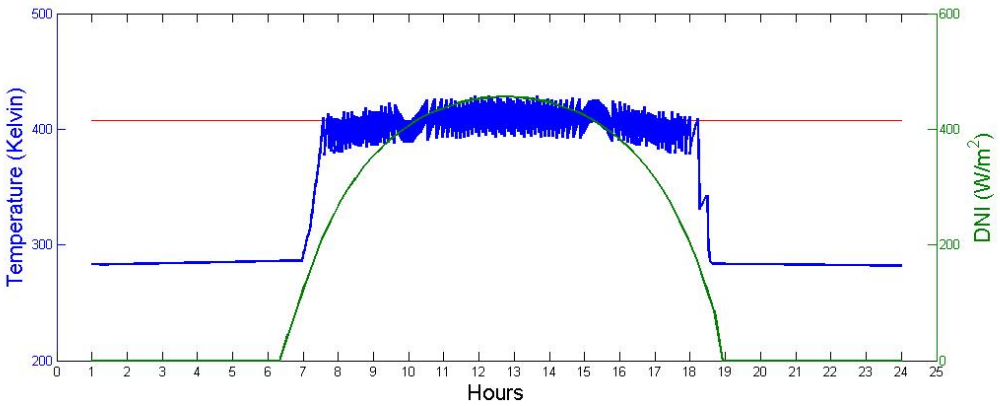

Figure 5.4. Daily irradiation and collector output temperature in April.

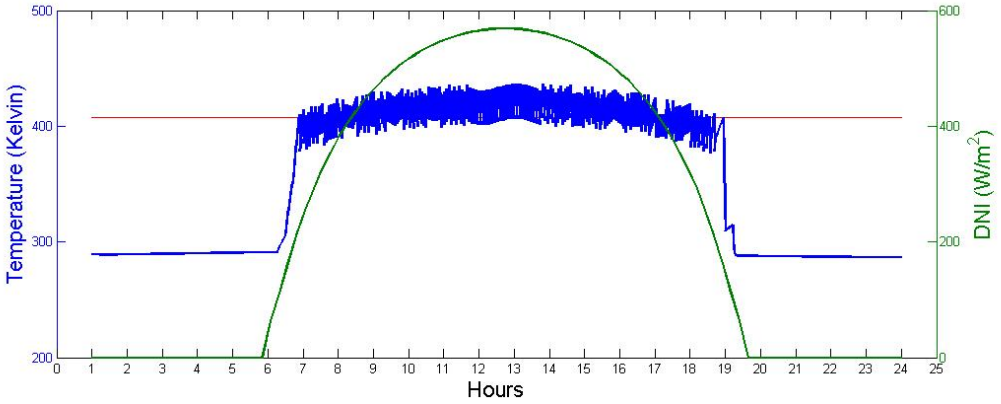

Figure 5.5. Daily irradiation and collector output temperature in May.

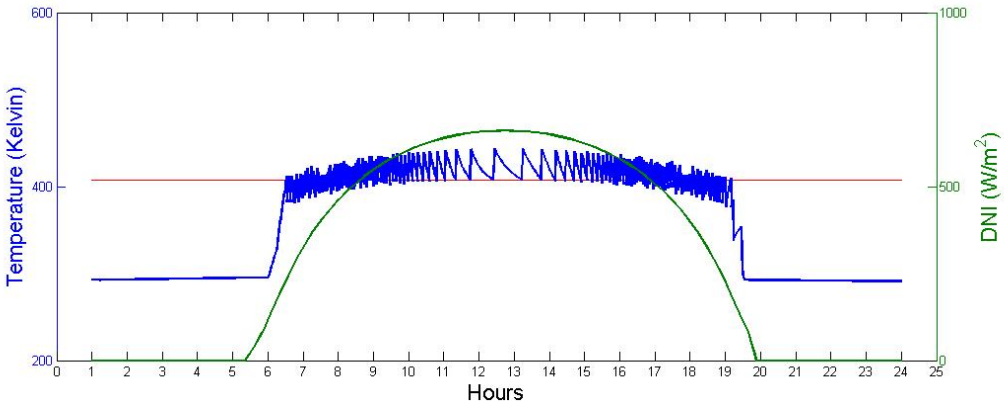

Figure 5.6. Daily irradiation and collector output temperature in June.

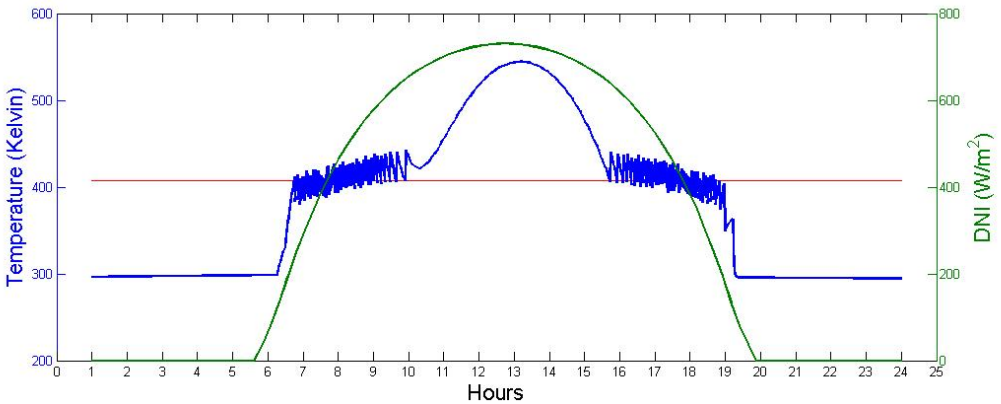

Figure 5.7. Daily irradiation and collector output temperature in July.

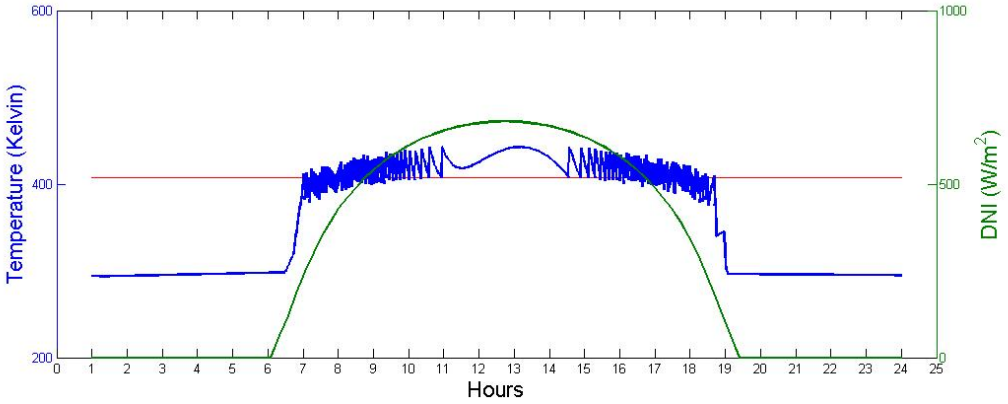

Figure 5.8. Daily irradiation and collector output temperature in August.

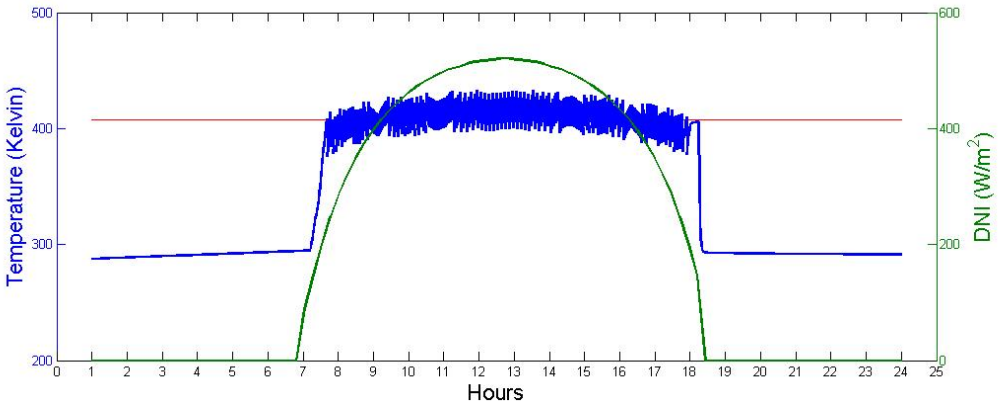

Figure 5.9. Daily irradiation and collector output temperature in September.

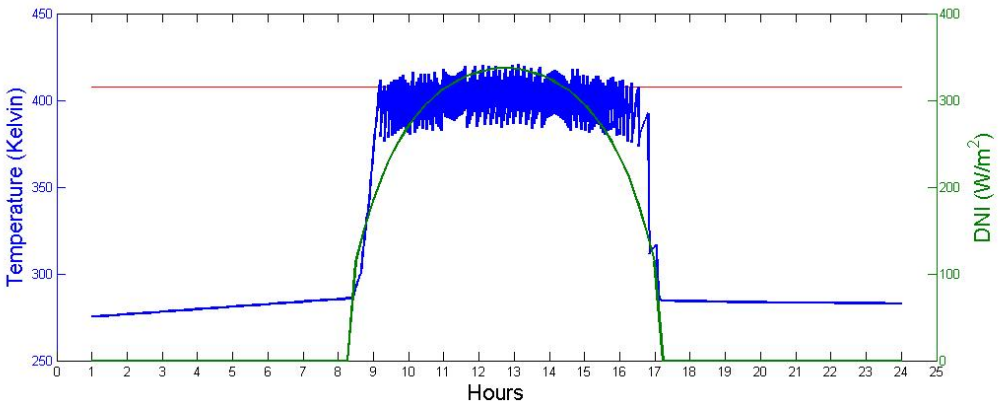

Figure 5.10. Daily irradiation and collector output temperature in October.

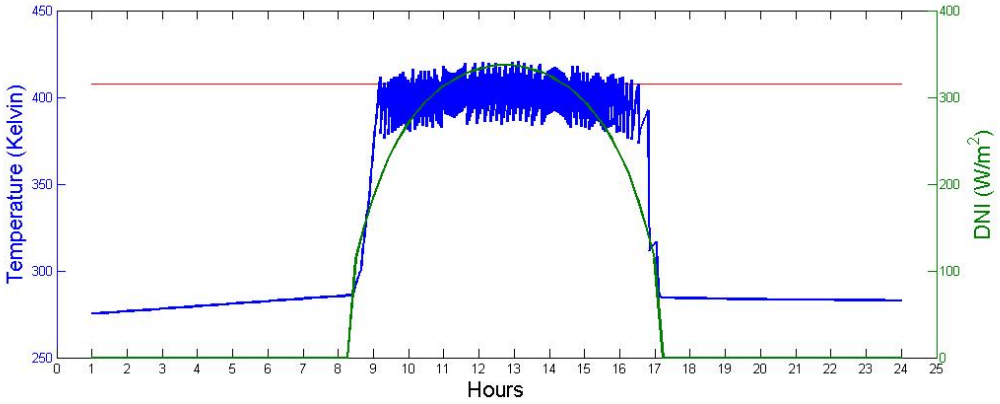

Figure 5.11. Daily irradiation and collector output temperature in November.

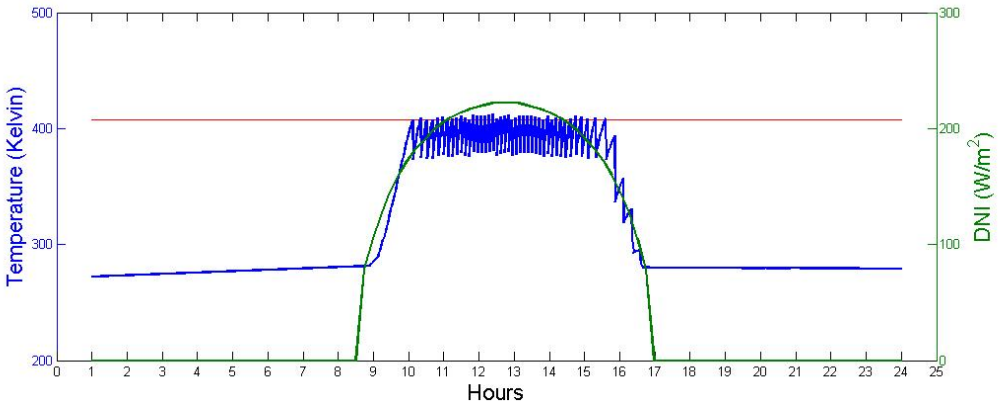

Figure 5.12. Daily irradiation and collector output temperature in December.

In July and August, there is a temperature increase during midday. In these hours, heat gain of the heat transfer fluid is more than heat input to the ORC. Therefore the ORC system can not use the whole energy gained from collector field. To avoid the degeneration of the HTF, and keep its temperature in its operation range, collector field should temporarily leave tracking the Sun. However during the other months, heat gain is barely satisfy the minimum set temperature for HTF, therefore ORC operates discontinuously. HTF circulates around itself in order to increase its temperature without going to evaporator, consequently operation time for ORC is limited. The annual performance of the system is shown in Table 5.2

Table 5.2. Daily performance of base case system with 200 m^2 collector area.

Month	Operation Time (min)	Daily work output (kWh)	System efficiency
January	63	10	0.027
February	86	13.65	0.030
March	196	31.12	0.040
April	299	47.48	0.053
May	457	72.58	0.060
June	589	93.54	0.064
July	609	96.20	0.064
August	565	89.00	0.065
September	360	57.17	0.059
October	190	30.17	0.048
November	133	21.12	0.043
December	42	6.67	0.021

5.1. Collector area sizing for power block

To maximize the system efficiency, simulation is repeated with different collector field area values. The results for fields of 150, 200 and 250 m^2 is shown in Table 5.3.

Increase in collector area to 250 m^2 increases the operation time for every month other than July and August. However the system efficiency for these months remains same. However the system efficiency for the months July and August decreases because extra the heat gain during the peak radiation times are can not be converted to extra work output. More increase in the area results with more decrease in the overall system efficiency.

Decreasing the collector field also only effect the system performance during the months July and August because with 150 m^2 collector area, the system can operate like as it does during other months. ORC works discontinuously while HTF is circulating only in the collector field to reach the required set temperature. Therefore we can

Table 5.3. Base ORC performance with different collector areas.

Month	min	kWh	eff.	min	kWh	eff.	min	kWh	eff.
January	63	10	0.027	79	12.54	0.027	47	7.46	0.027
February	86	13.65	0.03	108	17.15	0.32	64	10.16	0.031
March	196	31.12	0.04	245	38.9	0.047	147	23.34	0.047
April	299	47.48	0.053	372	59.08	0.053	224	35.57	0.053
May	457	72.58	0.06	570	90.53	0.06	343	54.47	0.06
June	589	93.54	0.064	669	106	0.058	442	70.2	0.064
July	609	96	0.064	661	104	0.055	475	75.44	0.066
August	565	89	0.065	628	99.74	0.058	425	67.5	0.065
September	360	57.17	0.059	449	71.31	0.059	271	43.04	0.059
October	190	30.17	0.048	236	37.48	0.047	142	22.55	0.047
November	133	21.12	0.043	166	26.36	0.043	100	15.88	0.043
December	42	6.67	0.021	53	8.41	0.021	31	4.92	0.021

conclude that 150 m^2 is optimum collector area for this ORC configuration in order to maximize the system efficiency. The change of work output with respect to collector field for three month (January, April and July) is shown if Figure 5.14.

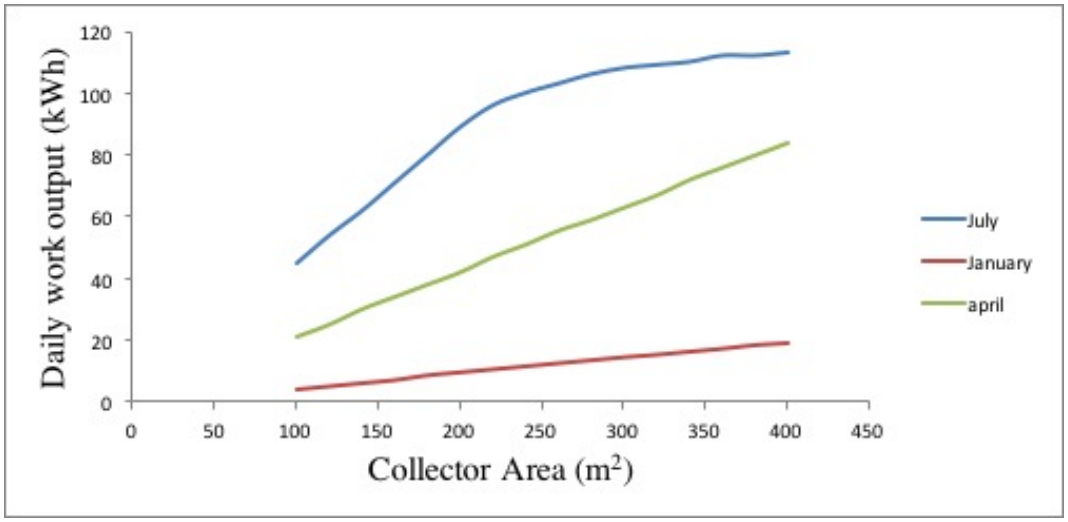

Figure 5.13. Effect of the solar field are on the cumulative work.

From figure it may be concluded that for July, optimum area for collector field is around 250 m^2. For this area work output is 103 kWh and with increasing the area

to its double, it only goes to 112 kWh. Because cycle operates nearly all day time, around 10 hours. So work output is maximized for this size of ORC system.

5.2. Effect of the HTF flow rate on daily performance

The fluctuations of the HTF temperature is the consequence of the rapid temperature drop of the HTF in the evaporator. To observe the system behavior, mass flow rate of HTF is varied while other parameters are constant and the collector field is set to 200 m^2. Increase in mass flow rate of the system reduce the temperature drop of HTF in the evaporator however it also decrease the temperature difference between inlet and outlet of the collector. As a result HTF fluid temperature varies more smoothly during day. The overall system work output remained same neglecting the very small amount of efficiency decrease.

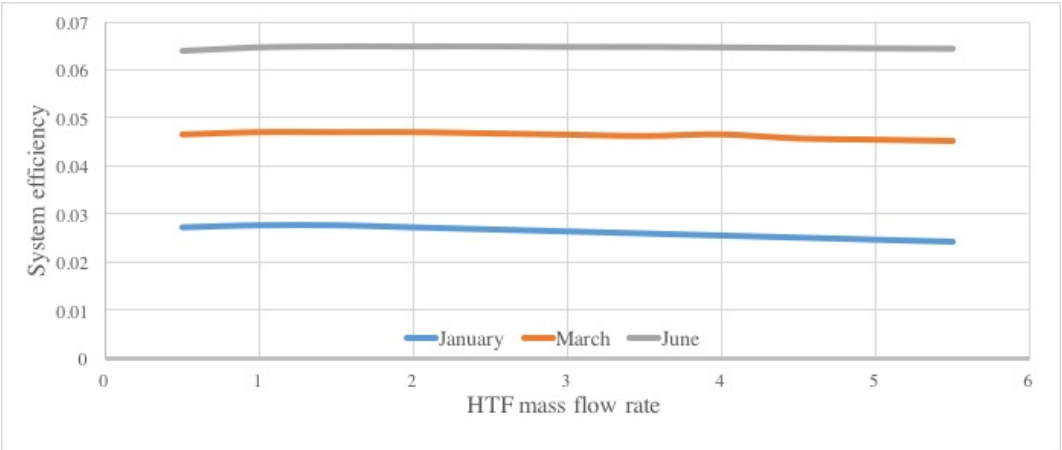

Figure 5.14. Effect of the solar field are on the cumulative work.

5.3. Effect of the evaporation pressure on daily performance

Increase in evaporation pressure has a positive effect on the system efficiency and work output. Given constant condensation pressure, pressure ratio of the cycle increases with the increase of the evaporation pressure and expander can generate more work however there are some practical limits for the pressure ratio of the cycle. In small scale applications expander axial turbines are not commercially available and pressure ratios of scroll expanders and radial expanders have lower values.

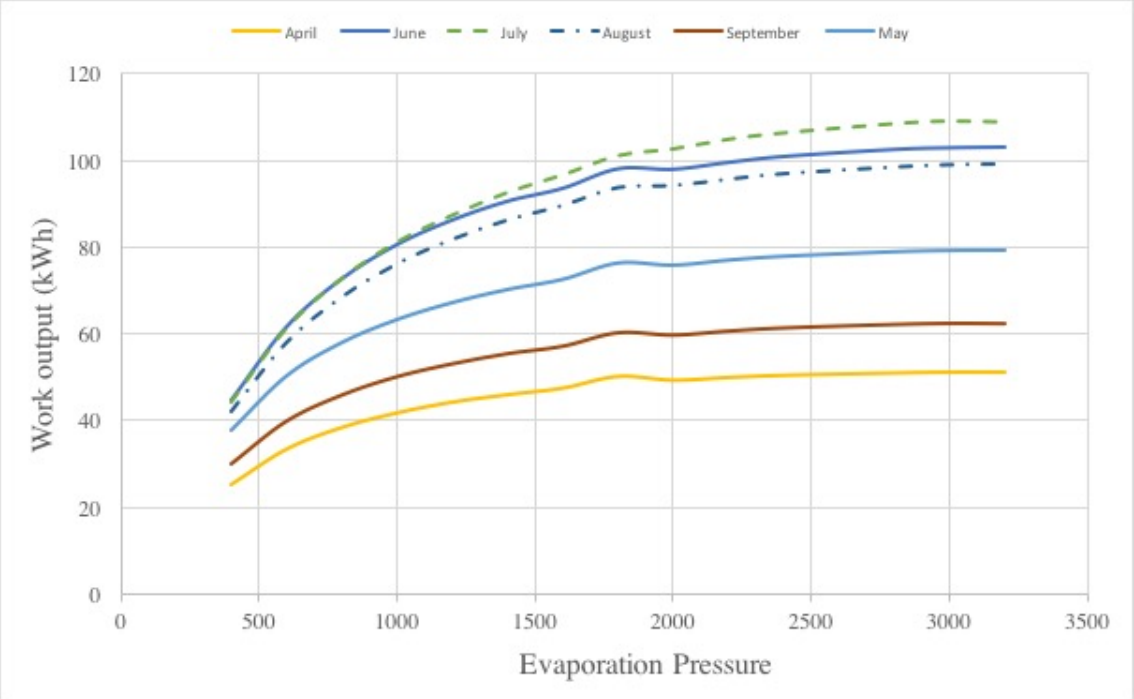

Figure 5.15. Variation of work output with change of working fluid mass flow rate.

When evaporation pressure increases, the evaporation temperature of the cycle also increases. For a given solar field area, the cycles with high pressure ratios are hard to be operated. Effect of the evaporation pressure for different months, between April and September and between October and March are shown in Figure 5.16 and Figure 5.15 respectively. It can be seen that for in January as an example month of cold season, there is an upper limit for pressure ratio due to high evaporation temperature which is hard to be provided by solar collector field. When evaporation pressure is more than 16 bar, the heat transfer fluid have to circulate longer times to reach necessary temperature for working fluid evaporation. However for July, higher evaporation pressures and temperatures can be achieved by abundant solar heat flux. However when pressure is further increased work output of the system converges to a certain value.

5.4. Effect of the thermal storage tank on the daily work output

To utilize the surplus energy gained during in the peak hours of the solar radiation a storage tank is implemented to system. Without a thermal storage tank, the system efficiency is 6.4 % with daily work output of 96.72 kWh. The ORC operation starts

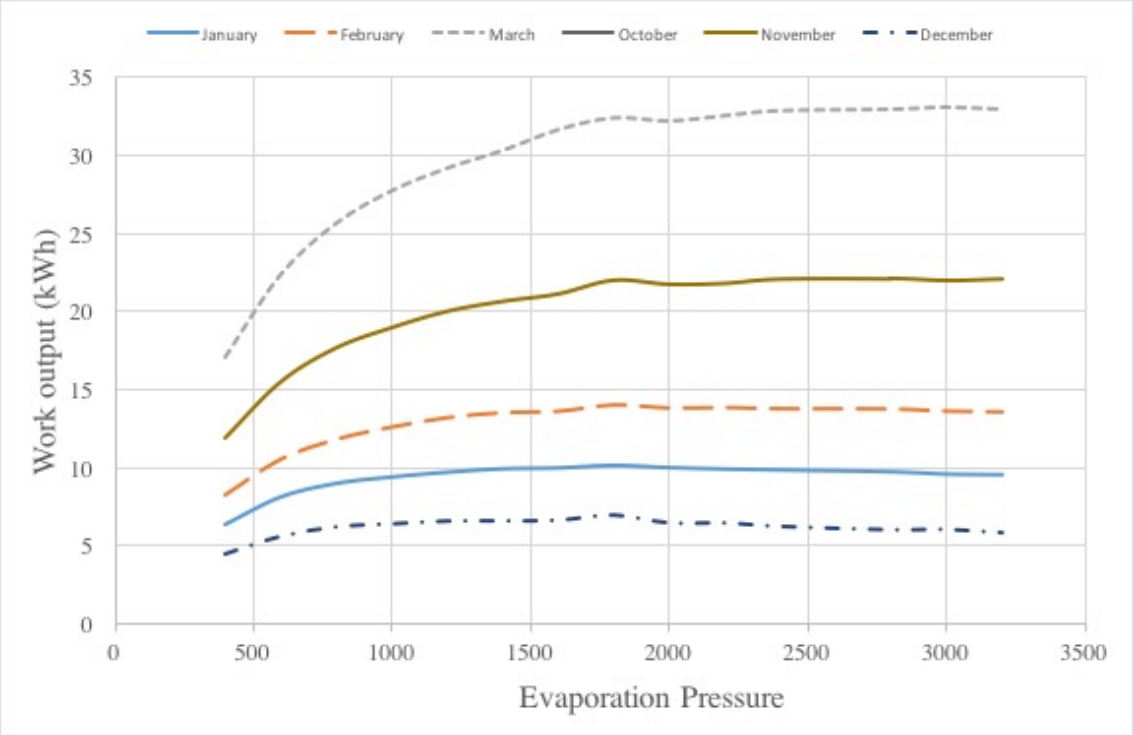

Figure 5.16. Variation of work output with change of working fluid mass flow rate.

around 7:09 and it stops at 17:18 for solar time of Istanbul. However if a storage tank with 4 m^3 volume is used, the overall efficiency increases to 7.18%. ORC starts to operate at the same time with the previous configuration the closing time for ORC is extended to 18.30. In this case total work output is 108 kWh. A 4 m^3 storage tank increased the overall efficiency by 12%.

5.5. Thermal Storage Tank Volume sizing for power block

Simulation is repeated with different tank volumes to see performance increase for the system due to extended operation hours. Tank volume has a optimum value at 8 m^3 for the plant as shown in Figure 5.19. When a small storage capacity is selected for the plant, the contribution of the storage will be clearly low. However if tank is over sized, due to high thermal inertia of the storage mass, the system can not increase the storage tank temperature to use it for discharging process in a typical day.

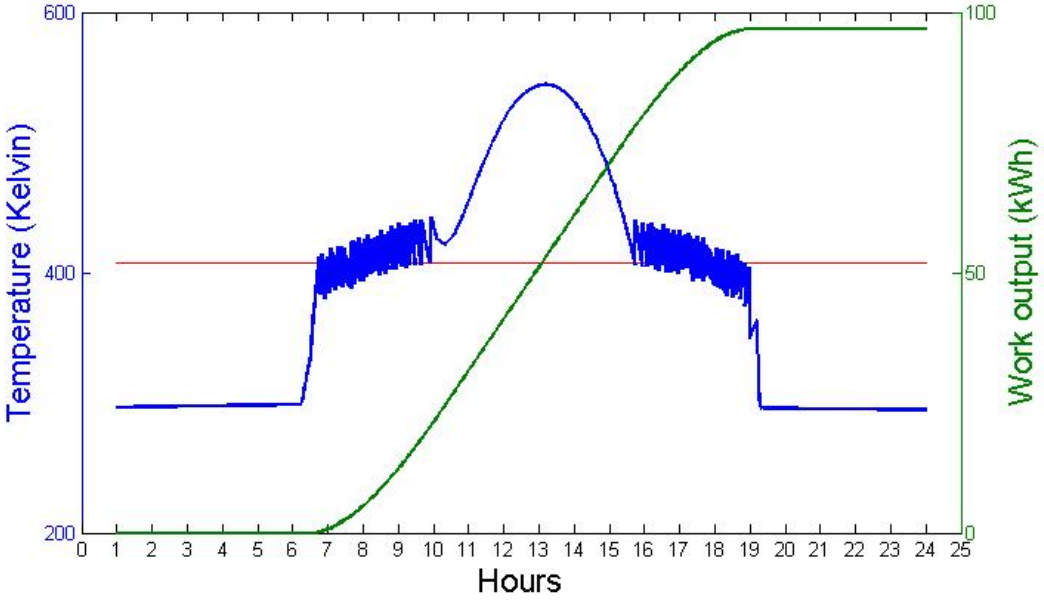

Figure 5.17. Performance of the base system without storage in July.

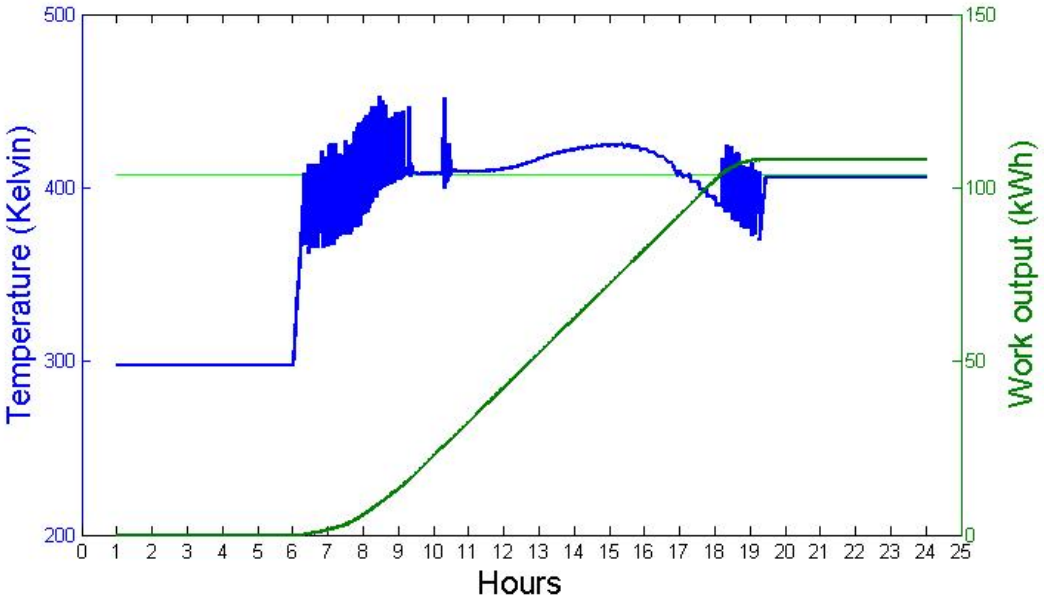

Figure 5.18. Performance of the base system with storage in July.

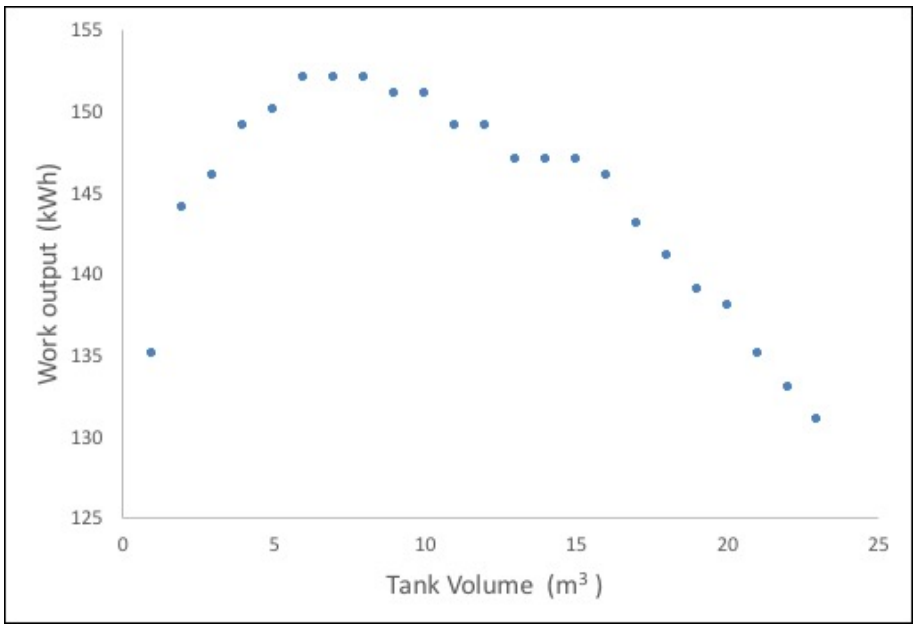

Figure 5.19. Effect of tank volume on the cumulative work.

when a small storage capacity is selected for the plant, the contribution of the storage will be clearly low. However if tank is over sized, due to high thermal inertia of the storage mass, the system can not increase the storage tank temperature to use it for discharging process in a typical day.

6. CONCLUSION

In this thesis work, a detailed thermodynamic model of organic Rankine cycle system and parabolic solar collectors has been developed and coupled with a single tank thermal storage system. The system and the collector field is sized according to organic Rankine cycle test setup in Bogazici University Kilyos Campus.

A thermal model of solar collector model is constructed to determine the output power and the temperature of the heat transfer fluid of the system for given dimensions, using thermal resistance method.

An organic Rankine cycle model is developed to calculate wok output of the system for given mass flow rates and pressures.

System is simulated under various seasonal conditions to observe effects such as collector area size, storage tank volume or evaporation pressure on the work output of the cycle.

REFERENCES

1. Mills, D., "Advances in solar thermal electricity technology", *solar Energy*, Vol. 76, No. 1, pp. 19–31, 2004.

2. "Department of Energy, USA", `http://energy.gov/eere/energybasics/articles/concentrating-solar-power-basics`, accessed at December 2016.

3. "Solar Thermal Electricity Global Outlook 2016", `http://www.greenpeace.org/international/Global/international/publications/climate/2016/Solar-Thermal-Electricity-Global-Outlook-2016.pdf`, accessed at January 2016.

4. "NREL CSP Projects Database", `https://www.nrel.gov/csp/solarpaces/`, accessed at January 2016.

5. Quoilin, S., *Sustainable Energy Conversion Through the Use of Organic Rankine Cycles for Waste Heat Recovery and Solar Applications.*, Ph.D. Thesis, University of Liège (Belgium), 2011.

6. "ORC World Map", `http://orc-world-map.org/analysis.html`, accessed at December 2016.

7. Orosz, M., A. Mueller, S. Quoilin and H. Hemond, "Small scale solar ORC system for distributed power", *Proceedings of SolarPACES*, 2009.

8. Freeman, J., K. Hellgardt and C. N. Markides, "An assessment of solar-powered organic Rankine cycle systems for combined heating and power in UK domestic applications", *Applied Energy*, Vol. 138, pp. 605–620, 2015.

9. Wang, M., J. Wang, Y. Zhao, P. Zhao and Y. Dai, *Thermodynamic analysis and optimization of a solar-driven regenerative organic Rankine cycle (ORC) based on*

flat-plate solar collectors, Vol. 50, pp. 816–825, 2013.

10. He, Y.-L., D.-H. Mei, W.-Q. Tao, W.-W. Yang and H.-L. Liu, "Simulation of the parabolic trough solar energy generation system with Organic Rankine Cycle", *Applied Energy*, Vol. 97, pp. 630–641, 2012.

11. Pehlivantürk, C., O. Özkan and D. K. Baker, "Modeling and simulations of a micro solar power system", *International Journal of Energy Research*, Vol. 38, No. 9, pp. 1129–1144, 2014.

12. "Greenway Web Site", `http://www.greenwaycsp.com/en/field-applications/mersin-5-mwth-solar-tower-plant.aspx`, accessed at December 2016.

13. TMMOB, "Turkiye Enerji Gorunumu 2016", `https://www.mmo.org.tr/kitaplar/turkiyenin-enerji-gorunumu-2016`, accessed at December 2016.

14. Antonelli, M., A. Baccioli, M. Francesconi, U. Desideri and L. Martorano, "Electrical production of a small size Concentrated Solar Power plant with compound parabolic collectors", *Renewable Energy*, Vol. 83, pp. 1110–1118, 2015.

15. "Power From The Sun", `http://www.powerfromthesun.net/Book/chapter08/chapter08.html`, accessed at December 2016.

16. John A. Duffie, W. A. B., *Solar Thermal Engineering of Thermal Processes*.

17. He, Y.-L., J. Xiao, Z.-D. Cheng and Y.-B. Tao, "A MCRT and FVM coupled simulation method for energy conversion process in parabolic trough solar collector", *Renewable Energy*, Vol. 36, No. 3, pp. 976–985, 2011.

18. Gu¨nther, M., M. Joemann and S. Csambor, *Advanced CSP Teaching Materials*, German Aerospace Centre, Institute of Solar Research, 2002.

19. Gil, A., M. Medrano, I. Martorell, A. Lázaro, P. Dolado, B. Zalba and L. F. Cabeza, "State of the art on high temperature thermal energy storage for power genera-

tion. Part 1—Concepts, materials and modellization", *Renewable and Sustainable Energy Reviews*, Vol. 14, No. 1, pp. 31–55, 2010.

20. Herrmann, U. and D. W. Kearney, "Survey of thermal energy storage for parabolic trough power plants", *Journal of Solar Energy Engineering*, Vol. 124, No. 2, pp. 145–152, 2002.

21. Pilkington Solar International, G., "Survey of thermal energy storage for parabolic trough power plants", *National Renewable Energy Laboratory*, Vol. SR-550-27925, 2000.

22. Pacheco, J. E., S. K. Showalter and W. J. Kolb, "Development of a molten-salt thermocline thermal storage system for parabolic trough plants", *Journal of solar energy engineering*, Vol. 124, No. 2, pp. 153–159, 2002.

23. Kolb, G. J. and V. Hassani, "Performance analysis of thermocline energy storage proposed for the 1 MW Saguaro solar trough plant", *ASME 2006 International Solar Energy Conference*, pp. 1–5, American Society of Mechanical Engineers, 2006.

24. Luzzi, A., K. Lovegrove, E. Filippi, H. Fricker, M. Schmitz-goeb, M. Chandapillai and S. Kaneff, "Techno-Economic analysis of a 10 MW e solar thermal power plant using ammonia-based thermochemical energy storage", *Solar energy*, Vol. 66, No. 2, pp. 91–101, 1999.

25. Rayegan, R. and Y. Tao, "A procedure to select working fluids for Solar Organic Rankine Cycles (ORCs)", *Renewable Energy*, Vol. 36, No. 2, pp. 659–670, 2011.

26. Tchanche, B. F., G. Papadakis, G. Lambrinos and A. Frangoudakis, "Fluid selection for a low-temperature solar organic Rankine cycle", *Applied Thermal Engineering*, Vol. 29, No. 11, pp. 2468–2476, 2009.

27. Bao, J. and L. Zhao, "A review of working fluid and expander selections for organic

Rankine cycle", *Renewable and Sustainable Energy Reviews*, Vol. 24, pp. 325–342, 2013.

28. Chen, H., D. Y. Goswami and E. K. Stefanakos, "A review of thermodynamic cycles and working fluids for the conversion of low-grade heat", *Renewable and sustainable energy reviews*, Vol. 14, No. 9, pp. 3059–3067, 2010.

29. Drescher, U. and D. Brüggemann, "Fluid selection for the Organic Rankine Cycle (ORC) in biomass power and heat plants", *Applied Thermal Engineering*, Vol. 27, No. 1, pp. 223–228, 2007.

30. Goswami, D. Y. and F. Kreith, *Handbook of energy efficiency and renewable energy*, Crc Press, 2007.

31. Incropera F, e., Dewitt DP, *Fundementals of heat and mass transfer*.

32. Kalogirou, S. A., "A detailed thermal model of a parabolic trough collector receiver", *Energy*, Vol. 48, No. 1, pp. 298–306, 2012.

33. Kalogirou, S. A., *Solar Energy Engineering*.

34. Ratzel, A., C. Hickox and D. Gartling, "Techniques for reducing thermal conduction and natural convection heat losses in annular receiver geometries", *Journal of Heat Transfer*, Vol. 101, No. 1, pp. 108–113, 1979.

35. Forristall, R., *Heat Transfer Analysis and Modeling of a Parabolic Trough Solar Receiver Implemented in Engineering Equation Solver*, Tech. rep., National Renewable Energy Laboratory, 2003.

36. Sloan M.; Mahoney A.R.; Mancini T.R.; Kolb, D. M. C. D. V., G.J.; Kearney, "Test Results: SEGS LS-2 Solar Collector", *NREL Report Database*, 2004.

37. Dudley, V. and G. Kolb, "Test results: SEGS LS-2 Solar Collector", *NREL Reports Database*, 1984.

38. “Spirax Sarco Web Page”, http://www.spiraxsarco.com/Resources/Pages/Steam-Engineering-Tutorials/steam-engineering-principles-and-heat-transfer/energy-consumption-of-tanks-and-vats.aspx, accessed at December 2016.

39. “Photovoltaic Geographical Information System (PVGIS)”, http://re.jrc.ec.europa.eu/pvgis/index.html, accessed at December 2016.

40. “Meteorology Department of Turkey, Official Website”, .